

CONTRACTOR REPORT

SAND92-7005
Unlimited Release
UC-261

Fatigue of Fiberglass Wind Turbine Blade Materials

John F. Mandell, Robert M. Reed, Daniel D. Samborsky
Department of Chemical Engineering
Montana State University
302 Cobleigh Hall
Bozeman, MT 59717

Prepared by Sandia National Laboratories Albuquerque, New Mexico 87185
and Livermore, California 94550 for the United States Department of Energy
under Contract DE-AC04-76DP00789

Printed August 1992

Issued by Sandia National Laboratories, operated for the United States Department of Energy by Sandia Corporation.

NOTICE: This report was prepared as an account of work sponsored by an agency of the United States Government. Neither the United States Government nor any agency thereof, nor any of their employees, nor any of their contractors, subcontractors, or their employees, makes any warranty, express or implied, or assumes any legal liability or responsibility for the accuracy, completeness, or usefulness of any information, apparatus, product, or process disclosed, or represents that its use would not infringe privately owned rights. Reference herein to any specific commercial product, process, or service by trade name, trademark, manufacturer, or otherwise, does not necessarily constitute or imply its endorsement, recommendation, or favoring by the United States Government, any agency thereof or any of their contractors or subcontractors. The views and opinions expressed herein do not necessarily state or reflect those of the United States Government, any agency thereof or any of their contractors.

Printed in the United States of America. This report has been reproduced directly from the best available copy.

Available to DOE and DOE contractors from
Office of Scientific and Technical Information
PO Box 62
Oak Ridge, TN 37831

Prices available from (615) 576-8401, FTS 626-8401

Available to the public from
National Technical Information Service
US Department of Commerce
5285 Port Royal Rd
Springfield, VA 22161

NTIS price codes
Printed copy: A04
Microfiche copy: A01

Distribution
Category UC-261

SAND92-7005
Unlimited Release
Printed August 1992

FATIGUE OF FIBERGLASS WIND TURBINE BLADE MATERIALS

J.F. Mandell, R.M. Reed, D.D. Samborsky
Montana State University
Bozeman, Montana 59717

Sandia Contract: 40-8875

ABSTRACT

Fatigue behavior for a variety of generic materials used in wind turbine blades has been explored. Coupon testing was carried out under constant amplitude tensile fatigue loading to beyond 10^7 cycles for most materials. Unidirectional materials performed close to expectations despite fiber misalignment. Materials with triaxial ($0/\pm 45$) reinforcement showed greater fatigue sensitivity than expected, but lifetime trends flattened at high cycles. The uniaxial and triaxial materials could be normalized to a single S-N lifetime trend for each case. Results include the effects of differing matrix materials, manufacturing methods, reinforcement structure, and ply terminations. Materials were supplied by Phoenix Industries and US Windpower.



TABLE OF CONTENTS

	<u>Page</u>
LIST OF TABLES.....	vi
LIST OF FIGURES.....	vi
INTRODUCTION.....	1
BACKGROUND	1
EXPERIMENTAL METHODS	4
Materials.....	4
Test Methods	5
RESULTS AND DISCUSSION	7
Unidirectional Materials.....	7
Triaxial Reinforcement.....	10
Ply Terminations.....	12
Delamination Growth.....	13
Comparison With Other Studies	15
SUMMARY.....	16
REFERENCES	15
TABLES	18
FIGURES.....	19
APPENDIX.....	52

LIST OF TABLES

	<u>PAGE</u>
TABLE 1 Description of Materials	18

LIST OF FIGURES

	<u>PAGE</u>
FIGURE 1 Typical S-N Data for Well Aligned Fibers, E-glass/Epoxy 0/90 Laminants, R = 0.1 [8].....	19
FIGURE 2 S-N Fatigue Data for SMC-R50 Chopped Glass Strand/Polyester, R = 0.1 [8].....	20
FIGURE 3 Typical S-N Fatigue Data for Style 181 Woven Glass Fabric/Polyester, R = 0.1 [5].	21
FIGURE 4 Geometry of Specimens With Ply Terminations and Joints	22
FIGURE 5 Test Coupon Geometry	23
FIGURE 6 Coupon Fabrication Schedule	24
FIGURE 7 Static Strength	25
FIGURE 8 S-N Data For Material B (Unidirectional)	26
FIGURE 9 Comparison of Normalized S-N Data for Unidirectional Materials A, B, and L	27
FIGURE 10 Modulus vs. Fractional Lifetime, Material B (Unidirectional)	28
FIGURE 11 Normalized Inverse Displacement vs. Fractional Lifetime, Material B (Unidirectional).....	29

FIGURE 12	(a) Typical Failures, Material A	30
12	(b) Typical Failures, Material B	31
12	(c) Typical Failures, Material C	32
FIGURE 13	Schematic of Edge Splitting in Unidirectional Materials	33
FIGURE 14	Material B S-N Data Fit With Eq.(1) with Cross-section Reduced to Account for 4 ^o Edge Split	34
FIGURE 15	S-N Data for Triax Materials M (Polyester) and N (Vinylester), [0/±45]	35
FIGURE 16	Normalized S-N Data for All Triax Materials	36
FIGURE 17	(a) Damage Growth and Failure, Materials F/G	37
17	(b) Failed Material N (0 ^o Directional)	38
17	(c) Materials H and J Showing Matrix Cracking and Failure	39
FIGURE 18	Cracking of 45 ^o Plies in Material N	40
FIGURE 19	Cracking Zone in Material N	41
FIGURE 20	Failure of 0 ^o Strand in a Cracking Zone, Material N	42
FIGURE 21	Initial Strain vs. Cycles to Failure, Unidirectional and Triaxial Materials	43
FIGURE 22	S-N Data for Material N Tested Transversely, [90/±45] vs. [0/±45]	44
FIGURE 23	Modulus vs. Fractional Lifetime, Material N Tested as [0/±45]	45
FIGURE 24	Modulus vs. Fractional Lifetime, Material N Tested Transversely [90/±45]	46

FIGURE 25	Surface Temperature vs. Fractional Lifetime, Materials H and J with Joint	47
FIGURE 26	S-N Data for Materials H and J with and without Joint in Gage Section (Stress Based on Net Cross- Section)	48
FIGURE 27	Schematic of Delaminations in Materials H/J	49
FIGURE 28	Typical Data for Delamination Total Length vs. Cycles at Three Stress Levels, Materials H/J.....	50
FIGURE 29	Delamination Crack Growth Rate Data for Materials H/J vs. Normalized Stress ($S_0 = 27$ ksi)	51

INTRODUCTION

The high cycle fatigue resistance of composite materials used in wind turbine rotor blades has been recognized as a major uncertainty in predicting the reliability of wind turbines over their design lifetime [1]. Blades are expected to experience 10^8 to 10^9 significant fatigue cycles over a 20 to 30 year lifetime, well beyond the cycle range of most aerospace structures on which much of the past research effort on composite materials has been focused. For the lower cost glass-fiber composites used in wind turbine blades, there exists neither an adequate data base at high cycles [1], nor an adequate lifetime prediction methodology proven for composite structures in general [2].

This report presents results from the first phase of a study of the high-cycle fatigue behavior of generic types of fiberglass materials used in wind turbines. This phase of the work was exploratory in nature, with fatigue test results up to to 40×10^6 cycles on a variety of materials prepared by U.S. blade producers. The results form the basis for future studies of carefully selected cases to be tested to higher cycles. (A single test to 10^8 cycles takes 50 to 100 days at frequencies in the range of 15 Hz, as used here.)

BACKGROUND

This section provides a brief overview of the literature on the fatigue of composite materials, with emphasis on the glass-fiber-based materials that are of primary concern with wind turbine blades. More detailed reviews of this subject can be found in References 1 - 7.

The fatigue behavior of composite materials is distinguished by several important general features [2, 3]:

1. Failure is usually progressive, resulting from the gradual accumulation and interaction of dispersed damage, rather than by the nucleation and growth of a dominant crack.
2. As damage accumulates, the constitutive relations of the material may change significantly.
3. A number of distinct damage modes can be identified, including fiber-dominated tension and compression, matrix-dominated cracking parallel to the fibers, and interlaminar cracking between plies. Some of these may produce failure directly, particularly fiber-dominated modes, while modes such as matrix cracking may have an indirect effect on failure by causing load transfer onto the fibers.
4. Under tensile loading the strains to produce matrix cracking (with thermoset resin composites) are generally well below those to produce fiber failure. As a consequence, in multidirectional composites, cracking tends to initiate first in domains (plies) where the fibers are at the greatest orientation relative to the maximum tensile stress. Cracking then

accumulates in these domains (such as 90° plies), followed by domains of lesser orientation (such as 45° plies). Delamination between plies may also occur at cut edges, ply terminations, or at the intersection of matrix cracks in adjoining plies. Finally, gross failure often occurs by fiber breakage in any domains oriented nearly parallel to the maximum stress (such as 0° plies). Under compressive loading the strains to produce matrix cracking in off-axis domains are often comparable to those for fiber-dominated failure, so damage development in a matrix-dominated mode may also produce gross failure.

5. Large-scale delamination between plies has been a significant failure mode for composite structures, particularly with out-of-plane loads. Classical linear elastic fracture mechanics has proven applicable to delamination problems under different modes of crack extension and for both static and fatigue loading.
6. Theoretical models for damage development and failure are under development, but no general approach to lifetime prediction for composites is widely accepted. Only delamination failures have a well-developed theoretical context through classical fracture mechanics.
7. Few results are available for lifetimes greater than 10^6 cycles for any composite systems.
8. Cumulative damage effects from varying load histories have been studied in only a few cases, and no general theoretical framework (such as linear damage laws) is accepted.

While these features are common to a broad range of fiber and matrix systems with continuous or chopped strand reinforcement, the actual sensitivity to fatigue loading depends strongly on the material system used, particularly the type of fiber and style of reinforcement (parallel aligned layers, woven, chopped, etc.). S-N lifetime data (maximum stress vs. cycles to failure) can follow a variety of trends [8,9], but the most simple and frequently observed are of the form

$$S/S_0 = 1 - b \log N \quad (1)$$

or $S/S_0 = N^{-(1/m)}$ (2)

where S is the maximum stress, S_0 is the single cycle strength, N is the number of cycles to failure, and m and b are constants. Equation (1) yields a linear S-N curve on a plot of S vs. $\log N$ while Eq.(2) is linear on a log-log plot. Equation (2) derives from integration of the Paris fatigue crack growth law

$$da/dN = A (K_{max})^m \quad (3)$$

where a is the crack length, K_{\max} is the maximum stress intensity factor (ΔK is more commonly used), A is a constant, and m is the same as in Equation (2).

Empirical findings are that S-N data for composites may show a better fit to either Equation (1) or (2) depending on the material system, and in many cases it is difficult to distinguish which is the more representative form. Composites with well-aligned fibers either parallel to the (uniaxial) load direction, or at some orientation, tend to follow Equation (1) closely, as do composites with multidirectional reinforcement where the lifetime is clearly dominated by one orientation [8,10]. Figure 1 shows such a data set for a 0/90 crossplied glass/epoxy composite. However, more complex cases, such as woven fabrics, and the chopped strand composites tend to have somewhat nonlinear S-N curves on a semi-log plot, and the most appropriate curve fit is unclear. Figure 2 (from Ref. 8) compares data from three laboratories for an automotive chopped glass strand/polyester composite, SMC R50. The data from different laboratories, with different test frequencies and specimen geometries, are in close agreement. This is one of the few sources with data approaching 10^8 cycles. The unfailed runout specimens (with arrows) still showed significant damage in the form of matrix cracks, and the existence of a fatigue limit is left uncertain. Either Equation (1) or (2) would fit the data adequately at moderate cycles depending on whether the high-cycle points are included in the fit. Woven fabric reinforcements (Fig. 3) show an even more nonlinear trend on a semi-log plot, with a steep curve at low to moderate cycles associated with delamination at the weave cross-over points [5], while the curves tend to flatten at higher cycles; significant high cycle data are not available.

The general trends of S-N data are also a function of constituent material properties in some cases. If S-N data sets are fit to Equation (1) in the range of 10^5 cycles, the following variations in the slope, b , of the normalized S-N curves are observed [8]:

1. In tension - tension fatigue, in well-aligned, fiber-dominated cases such as unidirectional strands and composites, the value of b is in the range of 0.1 for a broad range of glass fiber composites, so that the stress to fail the material in fatigue decreases by 10% of the static strength per decade (factor of 10) of increased lifetime. By comparison, carbon fiber systems show a slope of only 3-4%, and Kevlar is intermediate. The greater sensitivity of glass fiber-composites in tension appears to be the result of fiber - fiber contact damage during fatigue.
2. Matrix-dominated tensile fatigue, such as transverse tension, shear or $\pm\theta$ laminates show about 8-12% slopes, similar to the neat matrix materials.

3. Compression fatigue tends to be in the 8% range for both carbon and glass-fiber composites.
4. Multidirectional composites may follow a value of b approximately equal to that of the fiber direction unless there is enough load carried by the off-axis material to cause failure in the fiber direction layers when the lower strain-to-failure off-axis plies fail; then, the value of b may be similar to the matrix-dominated case [10]. Materials like woven fabrics, discussed earlier, may be fiber-dominated statically, but shift to matrix domination if the matrix cracking allows severe wear or movement of the weave [5].

Fatigue crack growth data for thermoset composites and neat resins tend to show very high exponents, m (Eq.3), compared with most metals, representing increased fatigue resistance since the curves converge approaching K_{Ic} . Values reported for m for both the neat matrix materials and opening mode delamination are often in the 10-20 range. For Mode II (shear) the exponents tend to be in the range of 10-12 [8,14,15].

EXPERIMENTAL METHODS

Materials

Materials were supplied by U.S. wind industry blade manufacturers, molded as flat sheets using preparation methods representative of blade manufacturing. This involved hand layup using nonwoven (stitched) E-glass fabrics having either unidirectional or triaxial ($0/\pm 45$) fibers. The triaxial reinforcement contained unidirectional layers stitched together, having differing amounts of 0° and $\pm 45^{\circ}$ material. The directions given refer to the angle of the fibers relative to the direction of the uniaxial stress that is applied to test specimens cut from the sheets, so that 0° indicates the fibers are approximately parallel-aligned in the direction of the applied stress.

Table 1 gives a description of each material used in this study (V_f is the volume fraction of fibers). The materials were intended to be as representative of wind turbine blades as possible, including typical fiber misalignments. However, to maintain reasonable specimen-to-specimen consistency, regions of material with greater than 4° fiber misalignment were excluded in preparing test specimens. This required rejecting material in local regions of only a few sheets and would not have been necessary at all except for the use of standard, narrow test specimens. These are expected to be dominated by local fiber misalignment to a much greater extent than would full-sized components.

The materials in Table 1 contain several different reinforcement styles, two generic types of matrix material (unsaturated polyester and unsaturated vinylester), and differing processing methods from the two manufacturers. Materials F, G, H and J also contain ply terminations to represent regions of blades that taper in thickness; these specimens are constructed symmetrically about the mid-thickness to minimize testing complications from nonsymmetrical cross-sections. Figure 4 depicts the geometry of these materials. F and G contain a double-ply drop-off from 6 to 4 plies in the center (a triax ply is a layer containing a $(0/\pm 45)$ structure). The distinction between F and G is that the 0° material faces toward the outside in F, while the $\pm 45^\circ$ material faces outside in G. Materials H and J contain more 0° material than F and G, and the geometry is that of a joint in the center two plies rather than a tapered thickness; again, H and J differ only in which side of the triax faces outward. The joint geometry proved more stable in testing than did the tapered thickness, which also failed away from the termination in most cases. These four materials were fabricated with the ply ends carefully cut and aligned; a region of matrix filled in the area at the edge of the cut ply, as shown in the schematics. Materials H and J were tested using two types of specimens, one containing the joint as shown in Fig. 4, and one without a joint in the gage section.

Test Methods

This phase of the study involved only tensile fatigue testing, and flat coupons of the general type shown in Fig. 5 were used, following ASTM D 3039-76 as closely as possible. The flat rectangular specimens were cut with a diamond-edged saw from larger sheets supplied by blade manufacturers. Tabs for gripping were bonded to the ends of the specimens, as shown, with an epoxy adhesive cured at room temperature or 140°F . (The original material sheets experienced exotherms in excess of 140° , and some were post cured at 140°F .) A variety of adhesives and tab materials were investigated, as indicated in the identification chart of Fig. 6. Most of the specimens were prepared with epoxy electrical vector board (Radio Shack Protoboard), which worked well in most cases. Problems were encountered with deterioration of the vector board at high cycles ($>10^7$), and other variations were attempted. A combination of 5 oz/yd² glass mat with an epoxy resin wrapping the tab area, plus vector board, and finally, a tapered aluminum tab bonded over the vector board (313 assembly, Fig. 6) eliminated tab deterioration. However, with unidirectional specimens, many high-cycle failures still occurred near the tab area, as described later. It was also found that sanding of the tabs to be flat and parallel was important, and was checked on precision flats within 0.002 in. in critical cases. One surface of the specimens was often very uneven, so the tab adhesive was applied with sufficient thickness to fill the low areas.

Tests were run in a 50 kip capacity MTS 880 servohydraulic testing machine using hydraulic grips. A constant-amplitude, force-control, sine-waveform loading was used in all cases. The frequency was

varied approximately inversely with the maximum stress level to maintain a constant load rate. The frequency at low cycles was a few Hz, varying up to 15 Hz for the highest cycle tests. This frequency range was the fastest possible without overheating of the specimens. As noted in Fig. 2, fatigue lifetime is not sensitive to frequency in the absence of thermal runaway hysteretic heating. This has been demonstrated over a broader range of frequencies in other studies [8]. The major effect of the frequency is in the strain rate sensitivity of fiberglass, which shows up primarily in low cycle tests [8]. The single-cycle tests in this study were run following a ramp waveform using a load rate consistent with that of the low-cycle fatigue tests, to avoid strain rate differences in the one-cycle data.

Strain measurement at higher cycles was a problem. Bonded strain gages failed, and fatigue extensometers did not always remain well seated. The cyclic stress-strain and modulus data given here were usually obtained by interrupting the tests and replacing the extensometer; thus, the cumulative strain, which was very small in cases where it was measured, was usually not included. Other test interruptions occurred due to power failures. These were common in very long tests, and the testing equipment did not generally overload the specimens significantly during shut-downs. Peak loads during shut-downs were recorded.

All tests were conducted in ambient laboratory air. This is generally low humidity with temperatures between 65 and 80°F.

RESULTS AND DISCUSSION

Detailed results from each static and fatigue test are given in the Appendix, including static strength; fatigue lifetime at designated maximum stress, S, and stress ratio, R, ($R = \text{min. stress/max. stress}$); frequency or static ramp rate; initial elastic modulus; maximum strain on the first cycle; and failure mode and position. Figure 7 gives the static tensile and compressive strength for each material, determined with ramp loading at a load rate consistent with low-cycle fatigue tests. The compressive tests are for unsupported gage lengths, which were sufficiently short to prevent elastic buckling. The compression behavior of these materials will be considered in detail in the next phase of the program. (It should be noted that the compressive strengths with either a greater thickness or with lateral support to prevent out-of-plane deformations could be considerably higher than those shown. With this test configuration, most compressive strengths were much lower than the tensile strengths.)

The following sections provide results and discussion of the fatigue behavior for each material system. Further details may be found in Reference 16.

Unidirectional Materials

Materials A, B, and L are unidirectional, loaded in the longitudinal (fiber) direction. A and B differ only in matrix material (polyester vs. vinylester); L is constructed with slight inherent fiber misalignment between strands and layers, and has a higher fiber content. Data are incomplete on L at this time, and additional data for A were obtained at the National Renewable Energy Laboratory with mechanical rather than hydraulic grips (not shown).

Figure 8 gives S-N data for material B. The arrows on the points at 40×10^6 cycles indicate run out tests that did not fail. Several aspects of Figure 8 are significant:

1. The data at higher stresses fall below Eq. 1 with a slope, b, of 0.1 (10%/decade). The data appear to be more nonlinear than those in Fig. 1, which are typical of well aligned glass fibers. These results are more similar to the chopped strands results in Fig. 2.
2. The power law fit of Eq. 2 is in good agreement with the data for an exponent, m, of 13.5.
3. There is no apparent effect of specimen width for the 1.0 and 2.0-inch-wide specimens tested.
4. The initial strain value given on the right, 0.68%, corresponds to the 20 ksi stress level. The actual strain increases slightly during the specimen lifetime.

Materials A, B, and L are compared in Fig. 9, with the maximum stress, S, normalized by the static strength, S_0 . Again, Eq.(2) with a power law exponent in the range of $m = 13.5$ fits the data well. Little difference between unidirectional Materials A, B, and L is noted, despite the differences in matrix material and manufacturing details. The vinylester matrix typically yields a slightly higher static strength (Fig.7, Material A vs. B), but little difference in fatigue, particularly at higher cycles.

Figure 10 gives the change in elastic modulus, E, normalized by the initial value, E_0 , as a function of the fractional lifetime for that particular specimen, n/N . The three specimens represented, tested at differing stress level, show a gradual decrease in modulus of 10 to 20% over the lifetime. Some of this apparent decrease is the result of edge splitting of the specimens, discussed in the following, which reduces the cross-section and decreases the apparent modulus (it is assumed in the stress calculation that the cross-sectional area remains constant). The modulus was determined from an extensometer which was periodically reattached to the specimen. Stiffness was also monitored by piston displacement. Figure 11 shows the inverse of the normalized displacement vs. n/N . This indicates a somewhat larger stiffness change than Fig. 10 for Specimens 21 and 38, apparently due to gradual cracking and delamination in the tab area of the gripped ends, effectively increasing the gage length. Specimen 22 shows greater effects of some actual grip slippage. Thus, extensometer measured stiffness values appear more meaningful despite extensometer attachment and edge splitting problems.

Figures 12 a, b and c show failed unidirectional specimens. Problems with failures in the tab area were common with unidirectional specimens, and clear tab failures were deleted from the plotted data. Edge splitting was also a common problem, as misaligned fibers were cut along the specimen edges, particularly notable with Material L (Fig. 12 c), but also a problem with A and B. Splits often occurred early in the lifetime, so that most of the lifetime was consumed with a reduced cross-sectional area and other complications such as nonsymmetry. The tabs often showed some delamination as well, particularly where the splits reached the tab area. The unidirectional materials showed some matrix cracking normal to the stress direction, particularly along the stitch lines; this was also observed in the run-out specimens.

The effects of the edge splits can be approximated by reducing the cross-section in the stress calculations to reflect the most severe splitting of about 4° off - axis, as shown in Fig. 13. Figure 14 shows the trend line produced for Material B if it is assumed that a split at 4° is present only in the fatigued specimens (as was observed), and then applying Eq. (1) with $b = 0.1$. This prediction provides a better fit to the data than Eq. (1) in Fig. 8, but Eq. (2) still seems to provide a better fit, particularly at high cycles.

As noted earlier, Eq. (1) has an empirical basis in a broad range of materials with well-aligned fibers, where $b = 0.1$ for E-glass strands and composites (Fig. 1). Equation (2) is generally applicable where the lifetime is associated with growing cracks, as in delamination studies [8], where Eq. (3) describes the crack-growth behavior. As noted later, delamination tests on Materials H and J produce a power law behavior following Eq. (3), with the same exponent, $m = 13.5$, which fits the unidirectional S-N data well. This implies that the lifetime of the unidirectional materials is dominated by the matrix-crack growth, edge-splitting process. However, the data in Fig. 8 are also not far from the expected trend of Eq. (1) with $b = 0.1$, and more high-cycle data will be required to adequately test either prediction.

Extrapolation to 10^9 cycles of the trend lines given in Eq.(8) for Eqs. (1) vs. (2) shows a great deal of sensitivity to the assumed model. The expected stress or strain level to produce 10^9 cycle failures is only half as great if Eq. (1) is assumed, as compared with Eq. (2). Again, more high-cycle data are required before a 10^9 cycle stress or strain level can be projected with any confidence.

Triaxial Reinforcement

Materials F/G, H/J, M and N contained $0/\pm 45$ layers of reinforcement with differing stacking sequence, relative amounts of 0 and ± 45 material, and strand sizes. These materials showed consistently poorer fatigue resistance than did the unidirectional materials. Figure 15 gives S-N data for Materials M and N,

with vinylester and polyester matrices, respectively. The vinylester matrix gives improvement in the static strength, but the fatigue data for the two matrices are indistinguishable. Both S-N data sets show a steep trend at high stresses, but flatten at stresses around 10 ksi.

Figure 16 compares S-N data for all of the triax materials on a normalized stress plot. Despite the differences in matrix, manufacturing, and percent 0^0 material, all of the data sets overlap, and all show a clear flattening trend at high cycles. The F/G and H/J data shown are for specimens without ply terminations (joints or tapers) in the gage section, or for specimens that failed away from the ply terminations. The effects of ply terminations will be discussed later.

The triax materials showed distinctly different failure patterns from the unidirectional materials. Figures 17 a, b and c show failed triax specimens. Generally, the $\pm 45^0$ layers fail separately and may delaminate from the 0^0 material. No significant tab problems were observed with most of these materials, and failures were usually in the gage section. The failure sequence usually showed cracking in the $\pm 45^0$ layers (Fig. 18), often associated with matrix cracks normal to the load in matrix-rich areas around the 0^0 material. Prior to total failure, local severe damage zones were observed to nucleate and grow. For F and G materials these appeared as in Fig. 17(a), while more distinct failures along stitch lines were seen in Materials M and N. These zones often, but not always, initiated at the edges. The failure zones in Materials M and N included cracks along the $\pm 45^0$ strands, and broken 0^0 strands right at the fabric stitch lines (Fig 20).

Figure 21 compares higher cycle strain data for the unidirectional and triax materials. The initial strains for the unidirectional materials were in the range of 0.8% to produce failure at 10^7 cycles, while for the triax materials the strain was in the range of 0.3 to 0.4%. The latter range is already well below the extrapolated unidirectional strains at 10^8 or 10^9 cycles, and so the triax results are very disappointing in terms of allowable strain levels. Also notable in Fig. 21 are data for the N triax tested in the transverse direction, ($90/\pm 45$). These failure strains are in the same range as for the 0^0 direction. It is apparent that all of the triax materials fail soon after the $\pm 45^0$ layers crack and are not dominated by the 0^0 layer strain capability. Figure 22 gives a comparison of 0^0 and 90^0 oriented S-N data for Material N.

An approximate prediction of what should happen when the $\pm 45^0$ layers fail can be obtained from classical laminate theory [16]. If the $\pm 45^0$ ply stiffnesses are then assumed to be zero, in Materials M and N, for example, the overall modulus should decrease by about 25%, raising the strain on the 0^0 material by a factor of 1.25. From Fig. 21, even with the extreme assumption of zero stiffness in the cracked plies, $\pm 45^0$ ply failure should not lead to the observed failure of the 0^0 layers at the lower strain levels. As noted earlier, carbon fiber composites fabricated from prepreg tend to follow the 0^0 ply fatigue trends under these conditions [10]. Thus, the triax performance in tension is much poorer than

expected either from experience with other composites or from simple calculations. Further study of this problem is required.

Modulus data for Material N are given in Fig. 23. The actual modulus reduction during cycling, presumably caused by cracking in the $\pm 45^\circ$ plies, is slightly less than the value of 25% obtained by completely deleting the $\pm 45^\circ$ ply stiffness. The corresponding increase in strain on the laminate is, then, slightly less than the predicted factor of 1.25. As expected, the triax tested in the transverse direction shows a much greater modulus reduction during cycling (Fig. 24).

Figure 25 gives the surface temperature change in selected H and J materials as a function of their fractional lifetime. Temperatures, measured with a small thermocouple, typically rose by the order of 10-20 $^{\circ}\text{C}$, then remained steady through most of the lifetime, finally increasing more significantly just before total failure, as more severe damage was observed. Specimen 92 showed a much earlier increase to high temperatures as the thermocouple was located near a point of severe damage (as in Fig. 19).

Ply Terminations

Materials F/G and H/J contained ply terminations and joints, respectively, as shown in Fig. 4. No significant difference was found as a result of the ply stacking configuration (0° 's facing outside vs. $\pm 45^\circ$'s facing outside) for either type of material, for static strength, fatigue life, or delamination growth. All of the F/G materials failed in fatigue in the thinner section, away from the ply termination area. Thus, the ply termination did not appear to affect the strength or fatigue life.

Materials H and J delaminated at the ply joint as described later. At low stress levels the delamination remained localized, and specimens either were run outs with no failure to 20×10^6 cycles, or else failure occurred near the joint. Tests were also run on materials H and J without a joint in the gage section. The S-N data for specimens with and without a joint are compared in Figure 26, where the stress values for the specimens with a joint are calculated based on the net cross-sectional area excluding the two plies with the joint. The S-N data show no significant difference between the materials with and without a joint involving one-third of the plies. The joint has no greater effect on the fatigue properties than the simple reduction in load bearing area at the joint. The localized delaminations at the joint on run-out specimens did produce some fine powder, apparently as a result of wear at the delamination surfaces, and one specimen with an arrested delamination eventually failed in this area. It is not known whether abrasion at such damage could produce more failures at higher cycles.

Delamination Growth

As noted above, Materials F and G were originally chosen to study the effects of ply terminations on lifetime, as well as to study the growth characteristics of delaminations originating at ply terminations. However, failures in fatigue for F and G occurred in the 4-ply half of the specimen, usually remote from the ply termination. The joint arrangement for Materials H and J (Fig. 4) was then selected to get around this problem; H and J also have a more structural triax fabric, with a higher 0° fiber content (Table 1).

The process of delamination development and growth followed the generally expected trends. As indicated in Figure 27, a matrix crack (or cracks) first formed across the end of the cut plies, normal to the load direction. Delaminations parallel to the ply interface then formed from the matrix crack, and gradually propagated along the specimen length. The delamination cracks in this case should be a combination of Modes I and II (opening and forward shear, respectively). Delaminations first form as shown in Fig. 27, Stage 2, and then usually develop into a full "H" geometry and propagate steadily (Stage 3). The value of the stress intensity factor, K, or energy release rate, G, for a given maximum stress should gradually decrease with increasing delamination length, and should then be approximately constant once the delaminations are significantly longer than the laminate thickness [17,18]. For long delaminations, the total G (sum of G_I and G_{II}) is delamination length independent, and is given by [18]

$$G = (S^2/4t^2)[1/(E_{LD} t_{LD}) - 1/(E_{LAM} t)], \quad (4)$$

where S is the maximum applied stress on the gross cross-section
 E_{LAM} is the elastic modulus of the original laminate
 t is the thickness of the original laminate
 E_{LD} is the elastic modulus of the uncut plies
and t_{LD} is the thickness of the uncut plies.

The value of G calculated for materials H and J for well established, long delaminations is $3.27 \times 10^{-5} S^2 \text{ kJ/m}^2$ (where S is in MN/m^2). This is the value of G at each delamination tip.

Figure 20 shows the delamination growth data for several stress levels. The maximum stress was held constant throughout each test, and the total delamination length (total of four cracks) was measured vs. cycles. The fatigue-crack-growth rate was then determined only for the part of the growth that was well established in geometry and with delamination lengths greater than the laminate thickness. Figure 29

gives the growth rate for the total delamination length average for each test vs. normalized stress, S/S_0 . S_0 is the one-cycle stress (27 ksi) at which the delamination grows unstably, corresponding to an average G_C of 6.56 in.lb./in.² (1.13 kJ/m²).

The data in Figure 29 follow a classic Paris Law pattern, with an apparent threshold at low stress, and power law trend following Eq.(3) up to S/S_0 approaching 1.0, where the cracks become unstable. The power law exponent shown on the plot is $m = 13.5$, which is typical of m values for delamination data for similar composites [8,14,15,19] [the exponent is half this value if Eq. (3) is expressed in terms of G instead of K]. Most studies have not carried delamination tests to a sufficiently low G level to establish a threshold condition for crack growth, but Ref. 19 clearly shows a threshold for glass fabric composites under Mode I loading. Most of the delamination fronts completely terminated growth for about 30×10^6 cycles for the lowest rate point on Fig. 29.

The results in Fig. 29 need to be expanded to fully explore delamination problems with this class of materials. However, the data appear to correlate in two respects with the in-plane coupon results given previously. First, the exponent, m , of 13.5 from Fig. 29 is the same value that fits the S-N data in Figs. 8 and 9. This implies that the tension-fatigue-lifetime trends for unidirectional materials may be dominated by matrix-cracking events, notably edge splitting and tab delamination. The life-determining events in these coupons with cut edges and imperfectly aligned fibers may not be fiber failure directly, but cross-section reduction, abrasion, and load redistribution associated with matrix-dominated cracking. This effect might not be as significant in actual components without cut edges and with greater size. Further high-cycle data in both small and large specimens are needed to explore this question adequately.

The second aspect of Fig. 29, which may correlate with coupon performance, is the apparent crack-growth threshold. The triax S-N trend shows flattening at low stresses, having the appearance of a fatigue limit (Fig.16). This appears to be associated with the strain level being sufficiently low so that matrix-dominated cracks do not propagate parallel to the fibers of the $\pm 45^\circ$ plies. This condition may be a result of the apparent threshold value of G required for matrix-dominated crack growth in Fig. 29. Unfortunately, the strain level where this condition is observed is relatively low, around 0.3%. While this could be an acceptable design limit in some cases, it would still be very beneficial if cracking in the $\pm 45^\circ$ layers did not lead to failure in the 0° layers, as discussed earlier. It is generally difficult to raise the strain capability of the off-axis layers in fatigue, but processes that reduce porosity could be helpful; changes from polyester to vinylester do not appear to significantly change the cracking process.

Comparison With Other Studies

Several wind-energy related programs in Europe have produced significant fatigue data in materials of the general type studied here [20-24]. Data for unidirectional fiberglass composites in tensile fatigue ($R = 0.1$) show failure strains in the 10^6 to 10^8 cycle range, which are very similar to those in this study, around 0.8% at 10^7 cycles [20, 21]. The S-N data for predominantly unidirectional material at $R = 0.1$ in Ref. 20 approximately follow Eq. (1) with $b = 0.1$, with the data falling slightly above the predicted lifetimes (with some uncertainty about the static test load rate effects). No fatigue limit is found out to 10^8 cycles. Data for spectrum loading (WHISPER spectrum) are reasonably predicted by a linear damage law combined with the constant amplitude results. However, testing at two stress levels tended to extend the life at the second (lower) level, contrary to linear damage expectations. Reversed loading ($R = -1$) produces lower failure stress levels, but is presumably related to the nature of any buckling constraints in compression.

Results in Ref. 22 were generally similar to those found here in trend and strain levels for unidirectional material at $R = 0.1$. Compression data and $R = -1.0$ data are generally at similar strains to those in Ref. 20, despite the use of an antibuckling device, which appeared to raise the static compressive values. Spectrum fatigue results (WHiSPX) showed approximate agreement with linear damage law predictions in tensile-dominated fatigue, but less agreement in compression [23].

With regard to the effects of vinylester vs. polyester matrix materials, data in Ref. 24 support the findings in the present study. Materials with woven roving and mat reinforcement showed some advantage to vinylesters over orthophthalic polyesters at high stresses (above where matrix cracking occurs on the first cycle), but S-N data ($R = -1.0$) for all matrix systems converged at lower stresses/longer lifetimes. This has also been observed in automotive SMC composites with various matrix modifications [8]. Data reported in Ref. 25 for flexural fatigue appear to show similar convergence at high cycles for vinylester and polyester matrices, but the vinylester showed a greater advantage at lower cycles than found in other data sets.

SUMMARY

The fatigue behavior has been explored for a variety of glass-fiber composite materials of generic types used in wind turbine blades, fabricated by blade manufacturers. Coupon testing has been carried out to over 10^7 cycles in constant amplitude tensile fatigue; higher cycles will be pursued in the next phase of the program for selected cases. Consistent-fatigue lifetime trends were found for the two main types of materials: unidirectional (tested in the fiber direction) and triaxial (reinforced with $0/\pm 45$ layers, mostly loaded in the 0^0 direction).

The unidirectional materials performed close to expected trends despite significant fiber misalignment; a power law trend appeared to provide the best fit to most of the data. This may imply that the lifetime is dominated by the matrix cracking along misoriented material, as the power law exponent correlates with the exponent obtained in ply delamination tests. Triaxial materials showed a more steep S-N data trend at higher stresses, which tended to flatten at low stress. Data from several material types with differing matrix (vinylester and polyester), percent 0° material, and manufacturing method could be normalized to a single S-N curve. Failure of the triaxial material appears to be dominated by cracking in the ±45° plies, which was not anticipated.

Data are also provided for changes in laminate stiffness and temperature during cycling. Modes of damage and failure are identified and related to the material structure. Ply terminations and joints did not have a significant effect on fatigue lifetime, but delaminations emanated from ply terminations at low-strain levels, and gross failure was observed at an arrested delamination in one case.

REFERENCES

1. "Assessment of Research Needs for Wind Turbine Rotor Technology," Report of the Committee on Assessment of Research needs for Wind Turbine Rotor Materials Technology, National Research Council, National Academy Press, Washington, D.C. (1991).
2. "Life Prediction Methodologies for Composite Materials," Report of the Committee on Life Prediction Methodologies for Composite Materials, National Materials Advisory Board, NRC, National Academy Press, Washington D.C. (1991).
3. K.L. Reifsnider, Ed., Fatigue of Composite Materials, Vol. 4 Composite Materials Series, Ed. R. B. Pipes, Elsevier Publishing Co., London (1991).
4. A.H. Chardon and G. Verchery, Eds., Durability of Polymer Based Composite Systems for Structural Applications, Elsevier Applied Science, London (1991).
5. J.F. Mandell, "Fatigue Behavior of Fiber-Resin Composites", Developments in Reinforced Plastics-2, G. Pritchard, Ed., Applied Science Publishers, London, p. 67 (1982).
6. R. Talreja, "Fatigue of Composite Materials," Technomic, Lancaster, PA (1987).
7. M.J. Owen, in Short Fiber Reinforced Composite Materials, ASTM STP 772 B. A. Sanders, Ed., ASTM, Phil. p. 64 (1982).
8. J.F. Mandell, "Fatigue Behavior of Short Fiber Composite Materials," Ch. 7, The Fatigue Behavior of Composite Materials, K.L. Reifsnider, Ed., Elsevier Science Publishing, London (1991).
9. G.P. Sendeckyj, "Life Prediction for Resin-Matrix Composite Materials," Ch.10, The Fatigue Behavior of composite Materials, K.L. Reifsnider, Ed., Elsevier Science Publishing, London (1991).
10. A. Rotem and H.G. Nelson, in Fatigue of Fibrous Composite Materials, ASTM STP 723, ASTM Phil., p. 152 (1981).
11. D.L. Denton, "Mechanical Properties Characterization of an SMC-R50 Composite," Proc. 34th Annual Tech-Conf., Reinf. Plastics/Composites Inst., SPI, New York, Paper 11 F (1979).

12. J.F. Mandell, D.D. Huang, and F.J. McGarry, "Tensile Fatigue Performance of Glass Fiber Dominated Composites," *Composites Tech. Rev.*, 3(1981)93.
13. S.S. Wang and E.S. -M.Chim, "Fatigue Damage and Degradation in Random Mat Short-Fiber SMC Composite," *J. Compos. Mat.*, 17(1983)114.
14. D.J. Wilkins, "A Comparison of the Delamination and Environmental Resistance of a Graphite-Epoxy and a Graphite-Bismaleimide," Naval Air Systems Command Technical Reports, NAV-GD-0037 (1981).
15. J.F. Mandell, "Fatigue of Fiberglass Wind Turbine Blade Materials," 10th ASME Wind Energy Symposium, Energy Sources Technology Conference and Exhibition, ASME, Houston (January 21, 1991).
16. R.M. Reed, "Long Term Fatigue of Glass Fiber Reinforced Composite Materials for Wind Turbine Blades," M.S. Thesis, Dept. of Chemical Engineering, Montana State University (1991).
17. S.S. Wang and H.T. Wang "Interlaminar Crack Growth in Fiber Reinforced Composites During Fatigue," NASA CR-165434 NASA-Lewis Research Center (1981).
18. T.K. Obrien, "Analysis of Local Delaminations and Their Influence on Composite Laminate Behavior," in Delamination and Debonding of Materials, ASTM STP 876, W.S. Johnson, Ed., ASTM, Phil., p. 282 (1985).
19. C. Bathias and A. Laksimi, "Delamination Thresholds and Loading Effects in Fiber Glass Epoxy Composite," ASTM STP 876, W.S. Johnson, Ed., ASTM, Philadelphia, PA, 1985, p. 217.
20. P.W. Bach, "High Cycle Fatigue Testing of Glass Fiber Reinforced Polyester and Welded Structural Details," ECN Report C-91-010, ECN, Petten, The Netherlands (1991).
21. R.H.F. Tikkemeijer and P.A. Joosse, "Fatigue of Wind Turbine Materials," NOVEM Contract 24.300/0550, NOVEM Utrecht, 3503 R.E. Utrecht, The Netherlands (1991).
22. Ch. W. Kensche and T. Kalkuhl, "Fatigue Testing of GL-EP in Wind Turbine Rotor Blades," Proc. European Community Wind Energy Conf., Madrid (1990).

23. Ch. W. Kensche, Institute for Structure and Design, DLR Stuttgart, Germany, personal communication (1991).
24. A.T. Echtermeyer, L. Buene, B. Engh, and O.E. Sund, "Significance of Damage Caused by Fatigue on Mechanical Properties of Composite Laminates," Proc. ICCM 8, Honolulu (1991).
25. P. Burrell, T. McCabe, and R. de la Rosa, "Cycle Test Evaluation of Various Polyester Types and a Mathematical Model for Projecting Flexural Fatigue Endurance," Proc. 41st Ann. Tech. Conf. Reinforced Plastic/ Composite Inst., Society of the Plastics Industry, Paper 7-D (1986)

TABLE 1 DESCRIPTION OF MATERIALS

FIBERGLASS MATERIALS TESTED

MATERIAL	V _f	PLY GEOMETRY	MATRIX	THICKNESS (INCHES)	LOAD DIRECTION	DESCRIPTION
A	0.30	[0] ₅	polyester	0.16	0°	12 oz unidirectional fabric
B	0.30	[0] ₅	vinylester	0.16	0°	12 oz unidirectional fabric
F	0.36	[(±45/0) _n] _s	polyester	0.19/0.28	0°	33 oz Triax (48% 0's, 26% +45's, 26% -45's) 6 plies reduced to four at central ply termination
G	0.36	[(0/±45) _n] _s	polyester	0.19/0.28	0°	Same as material F
H	0.37	[(±45/0) ₃] _s	polyester	0.25	0°	32 oz Triax (70% 0's, 15% +45's, 15% -45's) 6 plies with ply joint in central 2 plies
J	0.37	[(0/±45) ₃] _s	polyester	0.25	0°	Same as material H
L	0.50	[0] _n	polyester	0.13	0°	Non-woven uniaxial fibers
M	0.38	[0/±45] _n	vinylester	0.15	0°	Triaxial reinforcement (Same percentages as F)
N	0.38	[0/±45] _n	polyester	0.15	0°, 90°	Same as material M

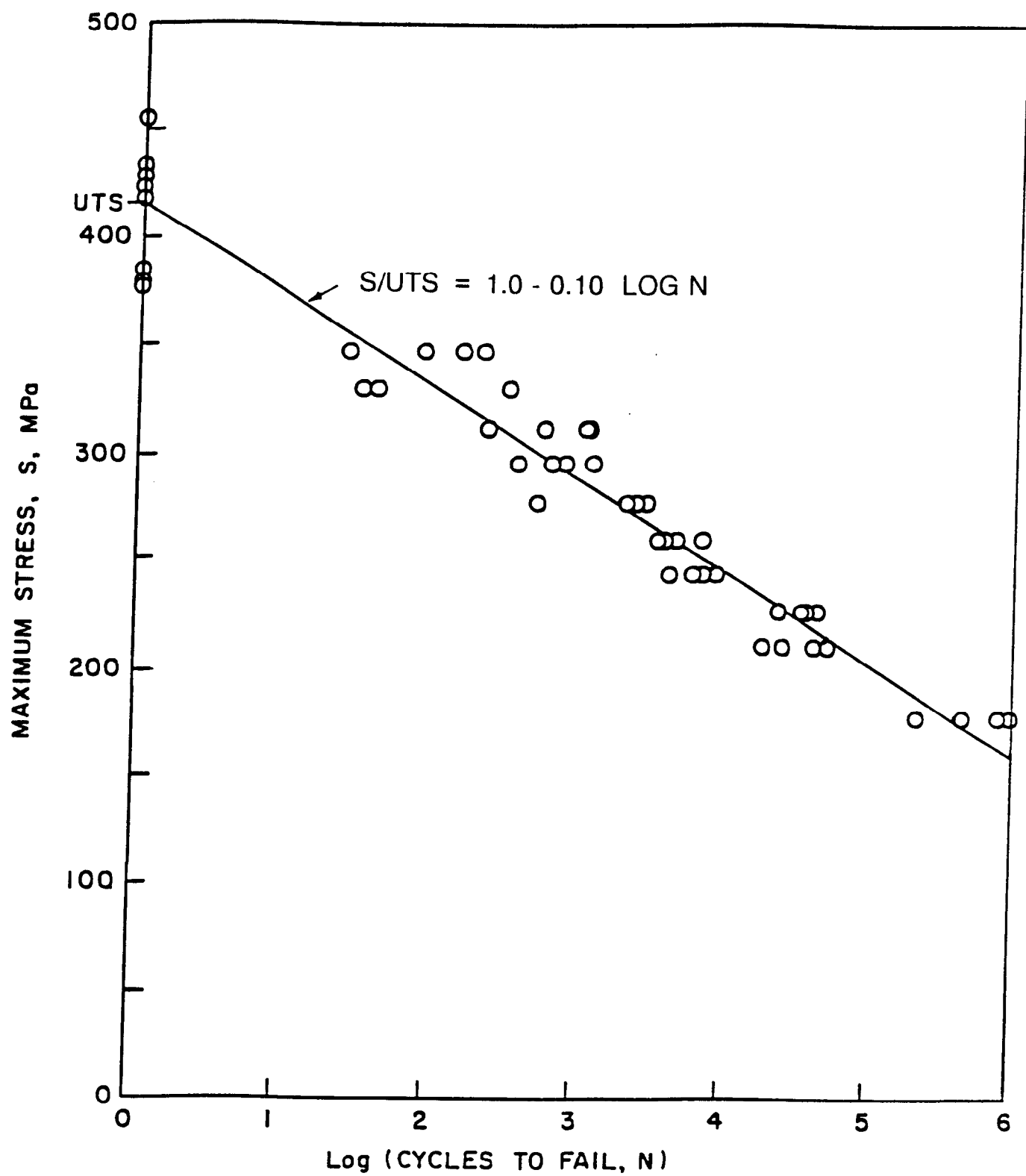


Figure 1 Typical S-N Data for Well Aligned Fibers, E-glass/Epoxy 0/90 Laminants, $R = 0.1$ [8]

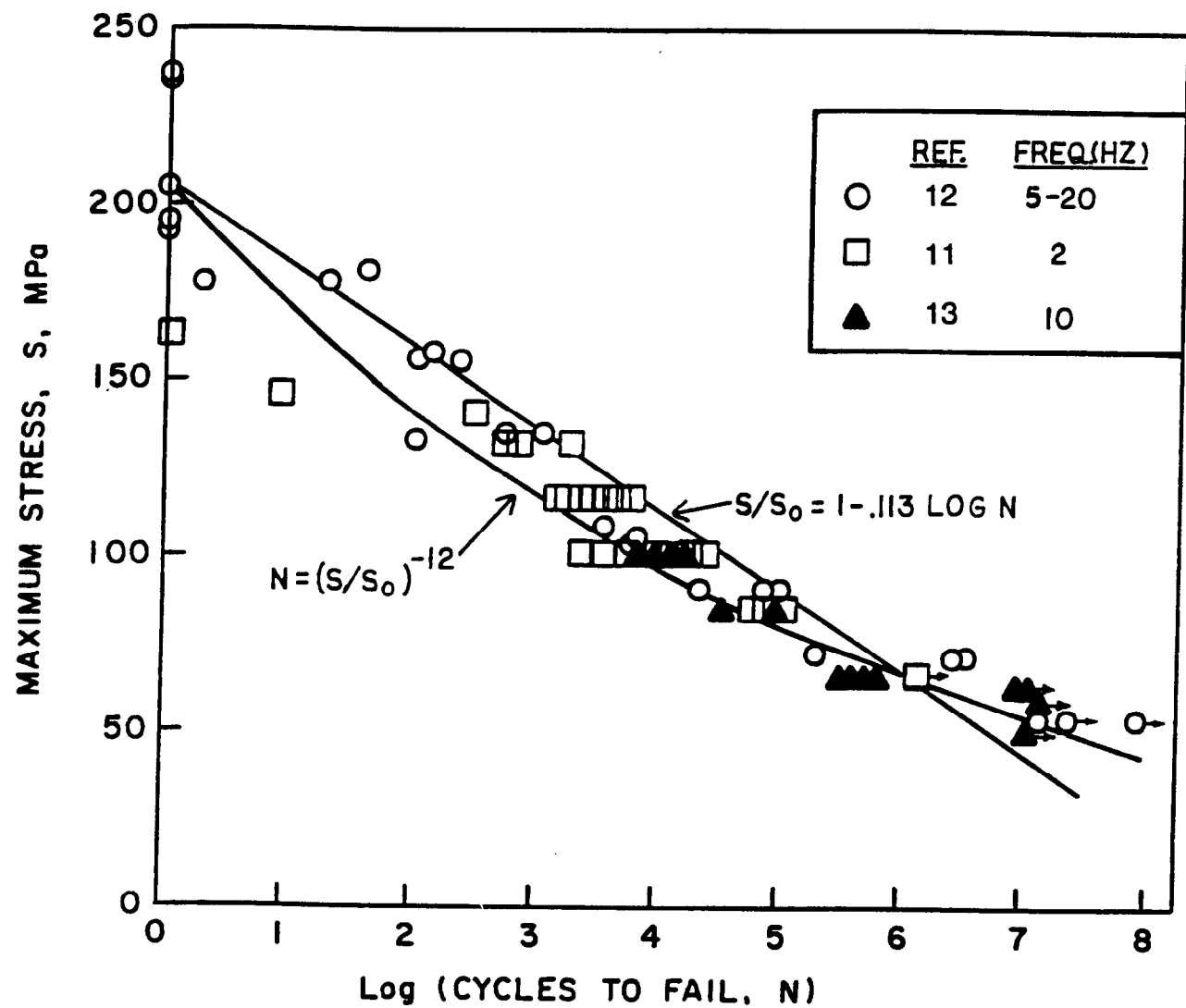


Figure 2 S-N Fatigue Data for SMC-R50 Chopped Glass strand/Polyester, $R = 0.1$ [8].

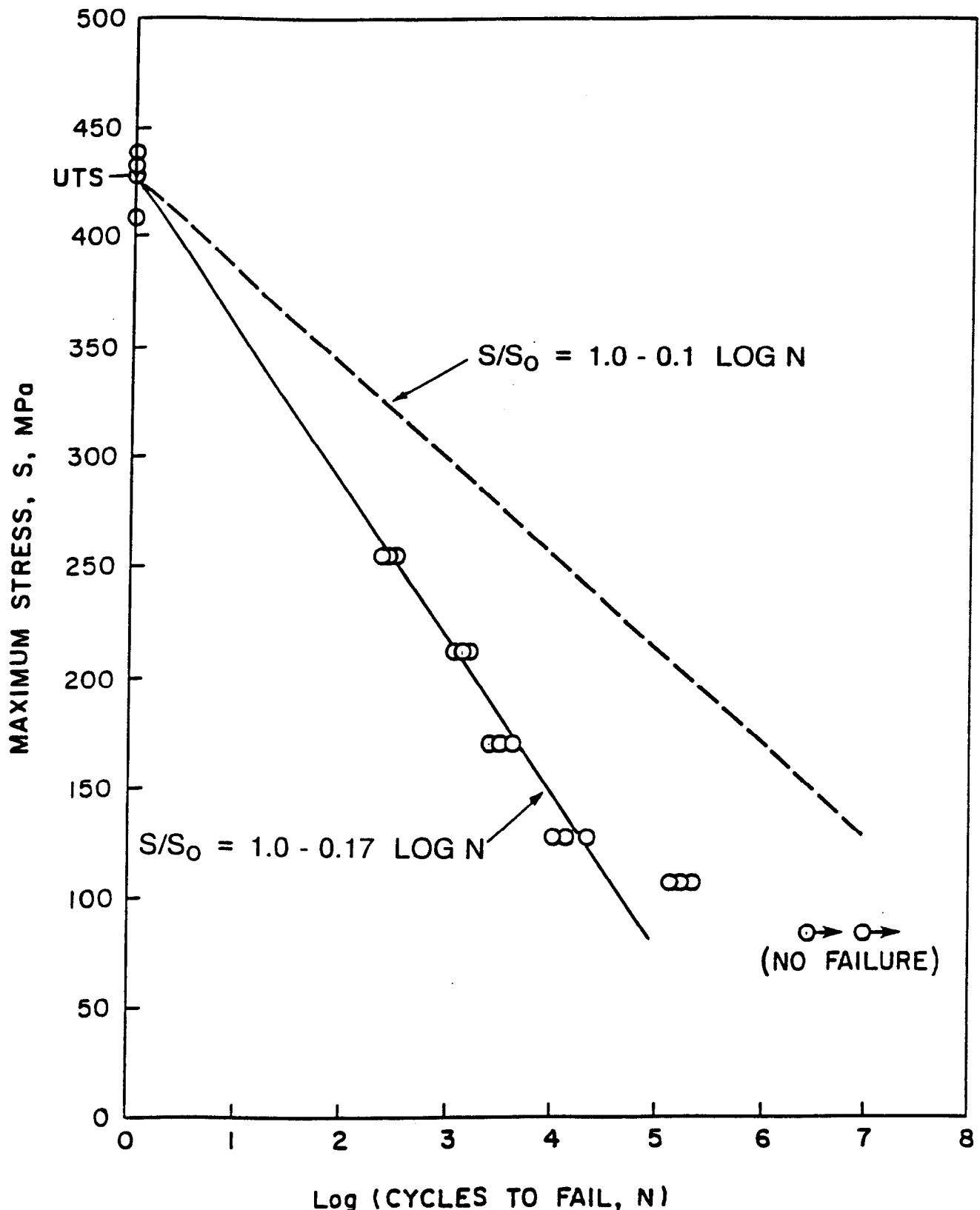


Figure 3 Typical S-N Fatigue Data for Style 181 Woven Glass Fabric/Polyester, $R = 0.1$ [5]

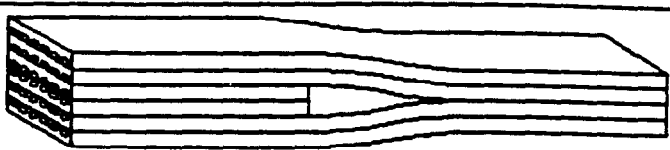
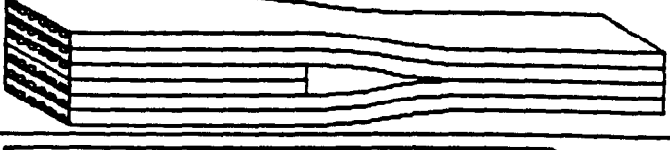
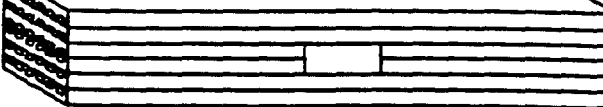
TEST MATERIAL	DESCRIPTION OF GEOMETRY TESTED	
	LOADING DIRECTION	
F	FOR EACH PLY 0 SIDE IN 45 SIDE OUT	
G	FOR EACH PLY 0 SIDE OUT 45 SIDE IN	
H	FOR EACH PLY 0 SIDE IN 45 SIDE OUT	
J	FOR EACH PLY 0 SIDE OUT 45 SIDE IN	

Figure 4 Geometry of Specimens With Ply Terminations and Joints

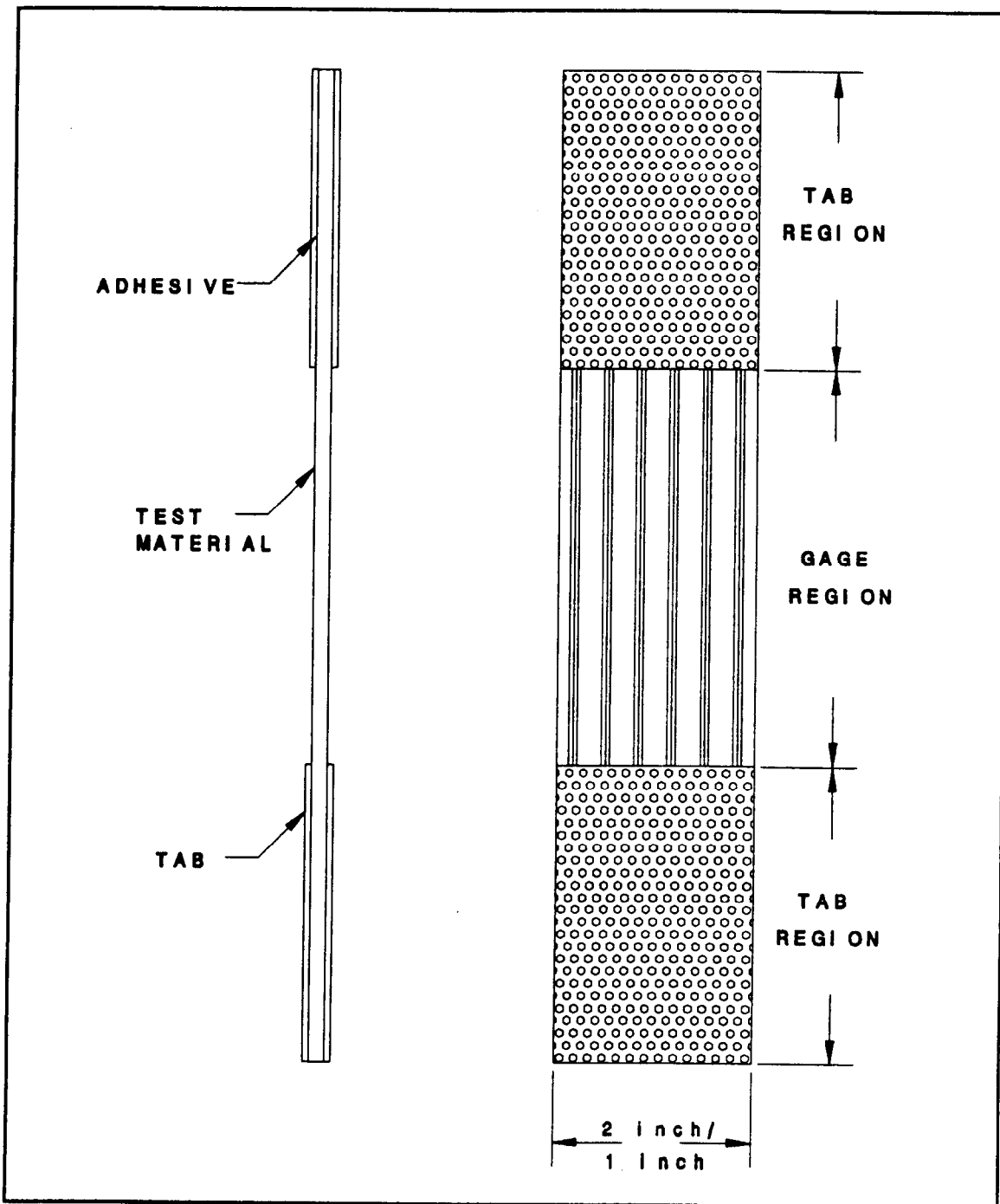


Figure 5 Test Coupon Geometry

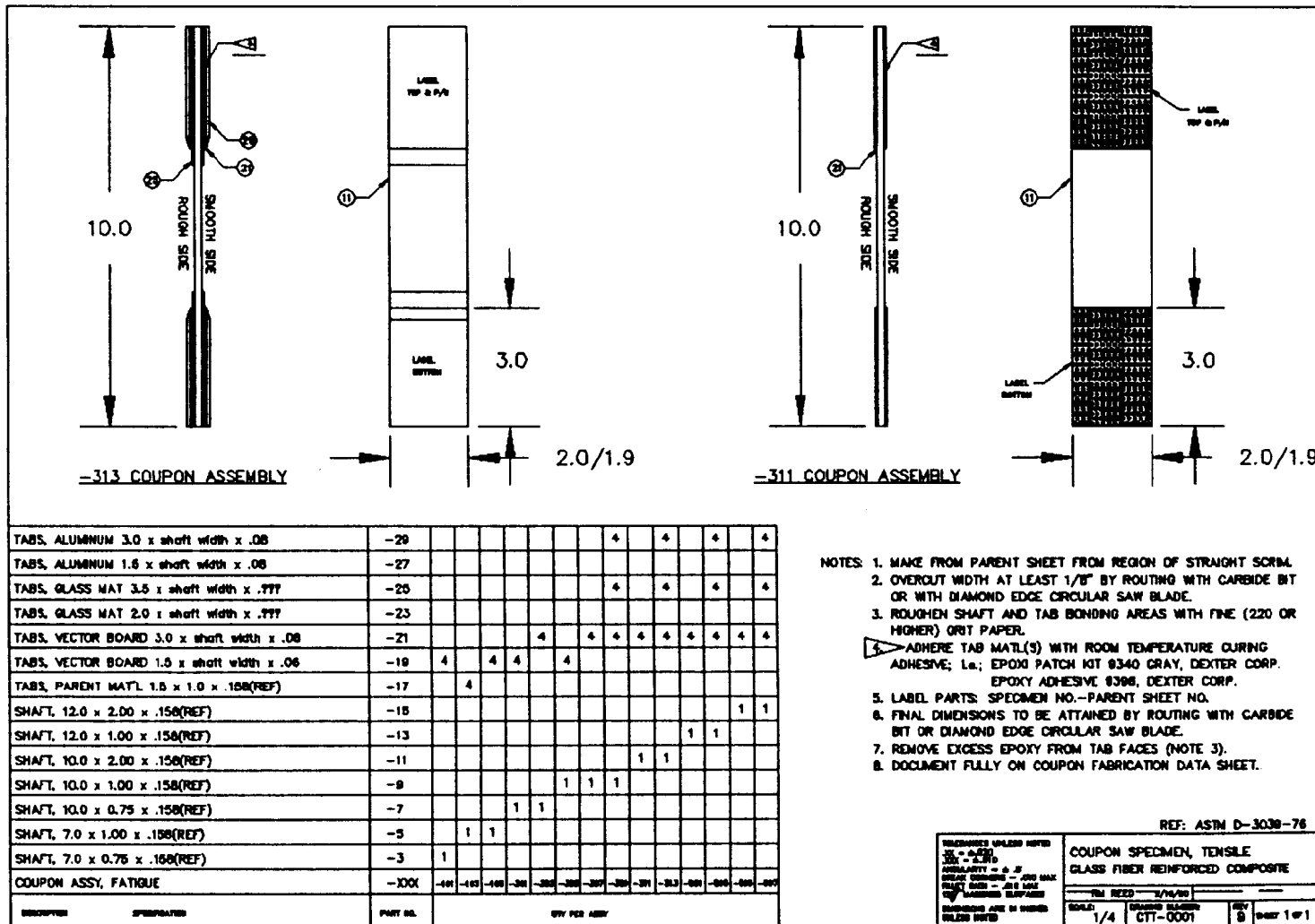


Figure 6 Coupon Fabrication Schedule

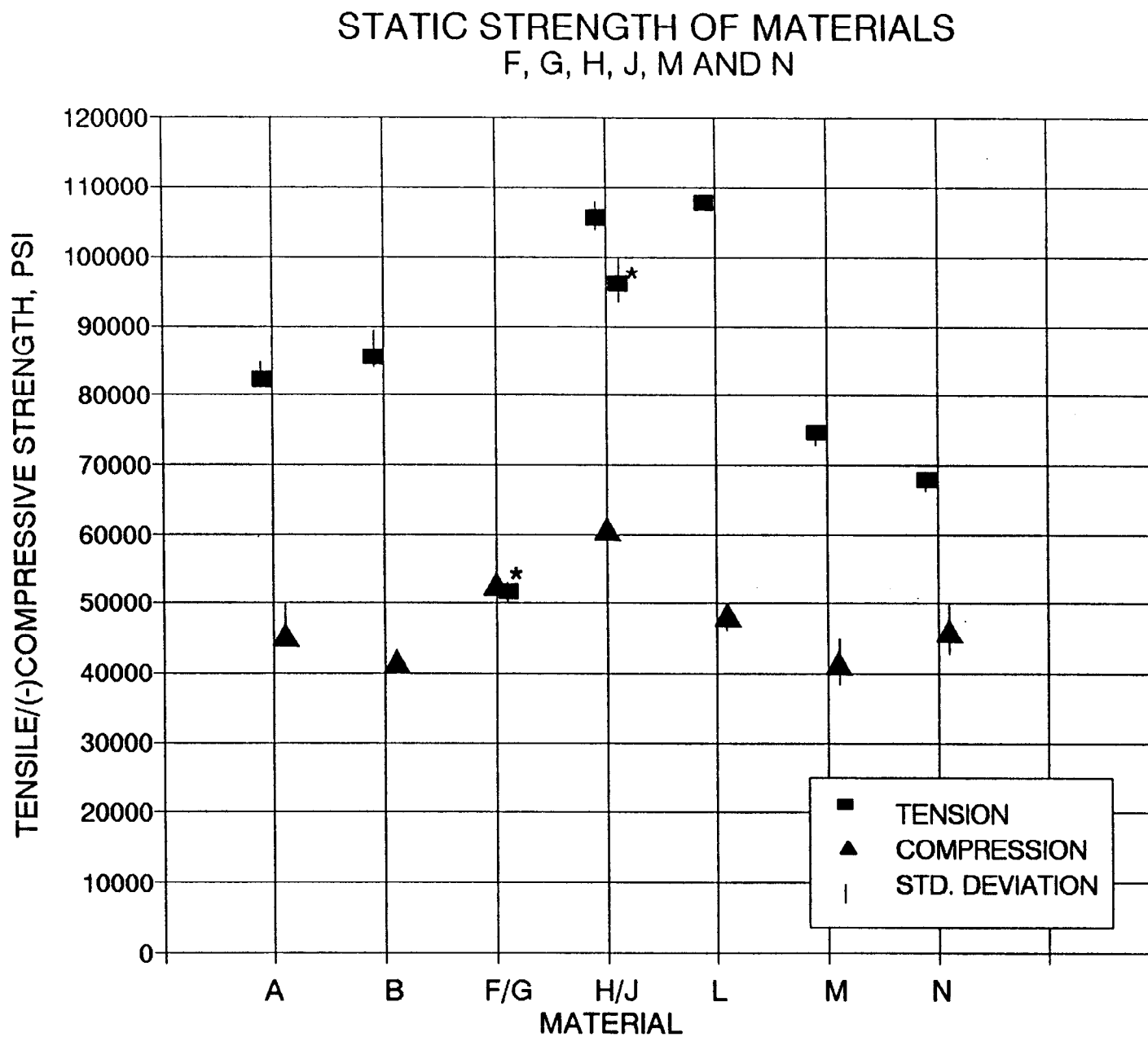


Figure 7 Static Strength, * With Ply Termination or Joint (Net-Section Strength)

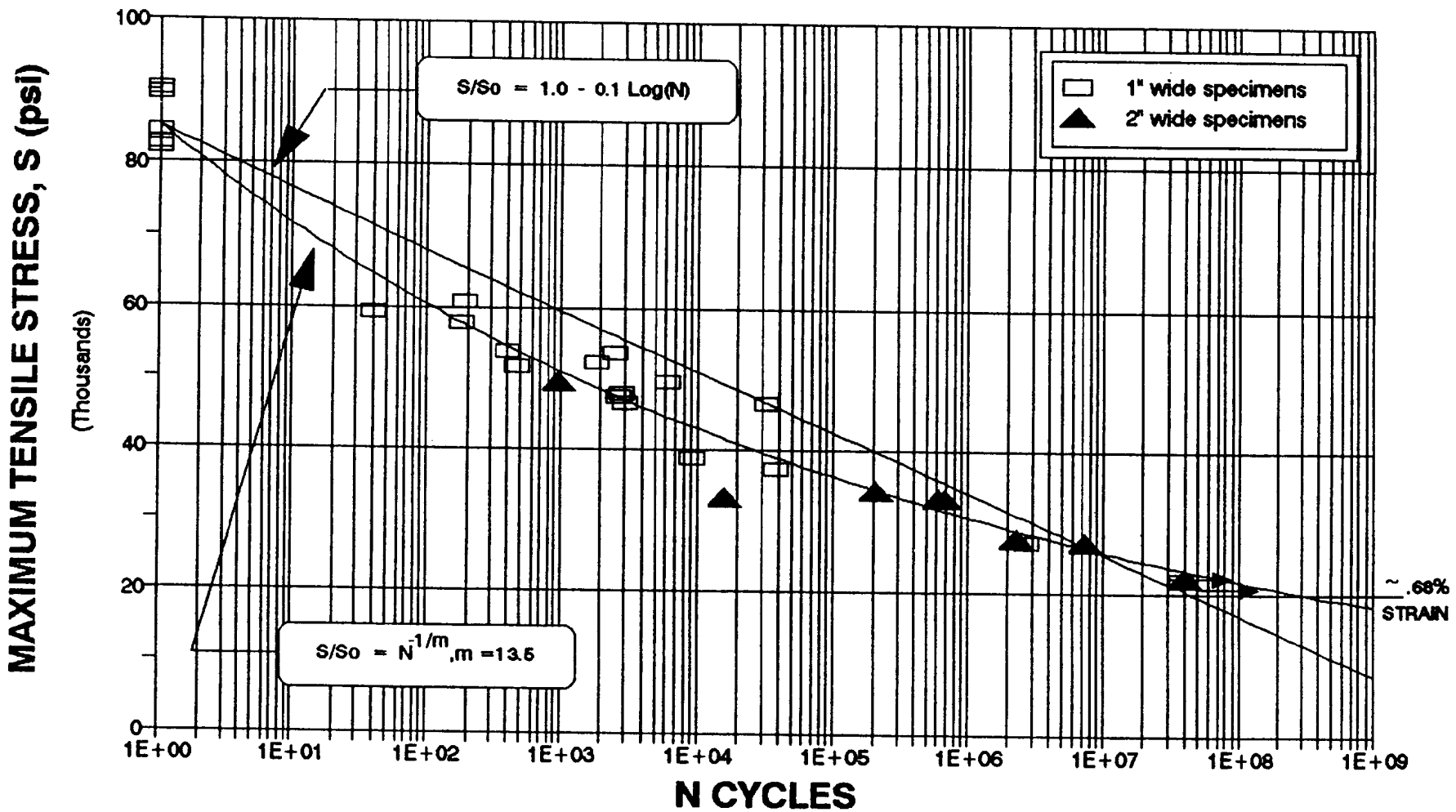


Figure 8 S-N Data For Material B (Unidirectional)

UNIDIRECTIONAL E-GLASS MATERIALS
A, B AND L AT R = 0.1

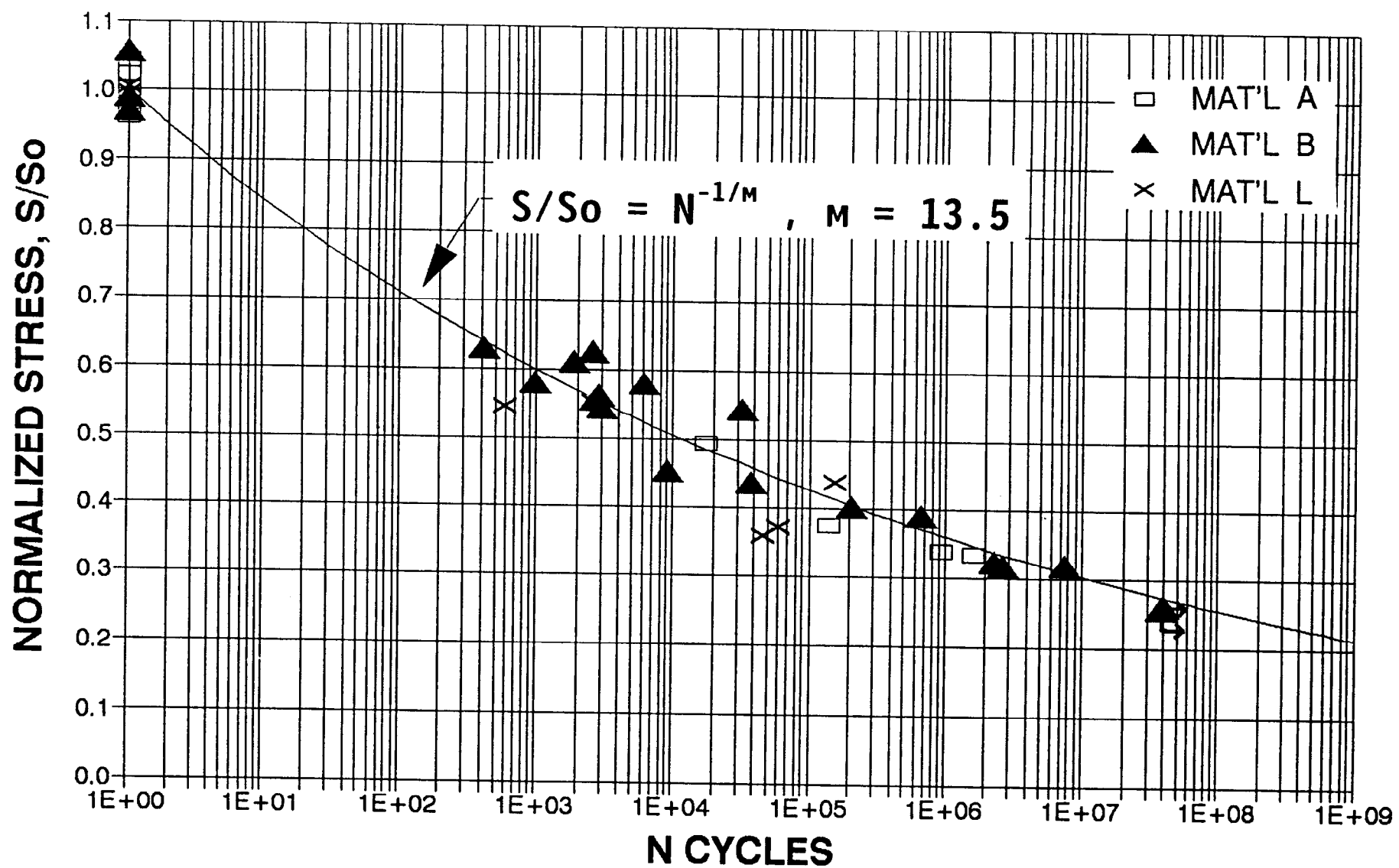


Figure 9 Comparison of Normalized S-N Data for Unidirectional Materials A, B, and L

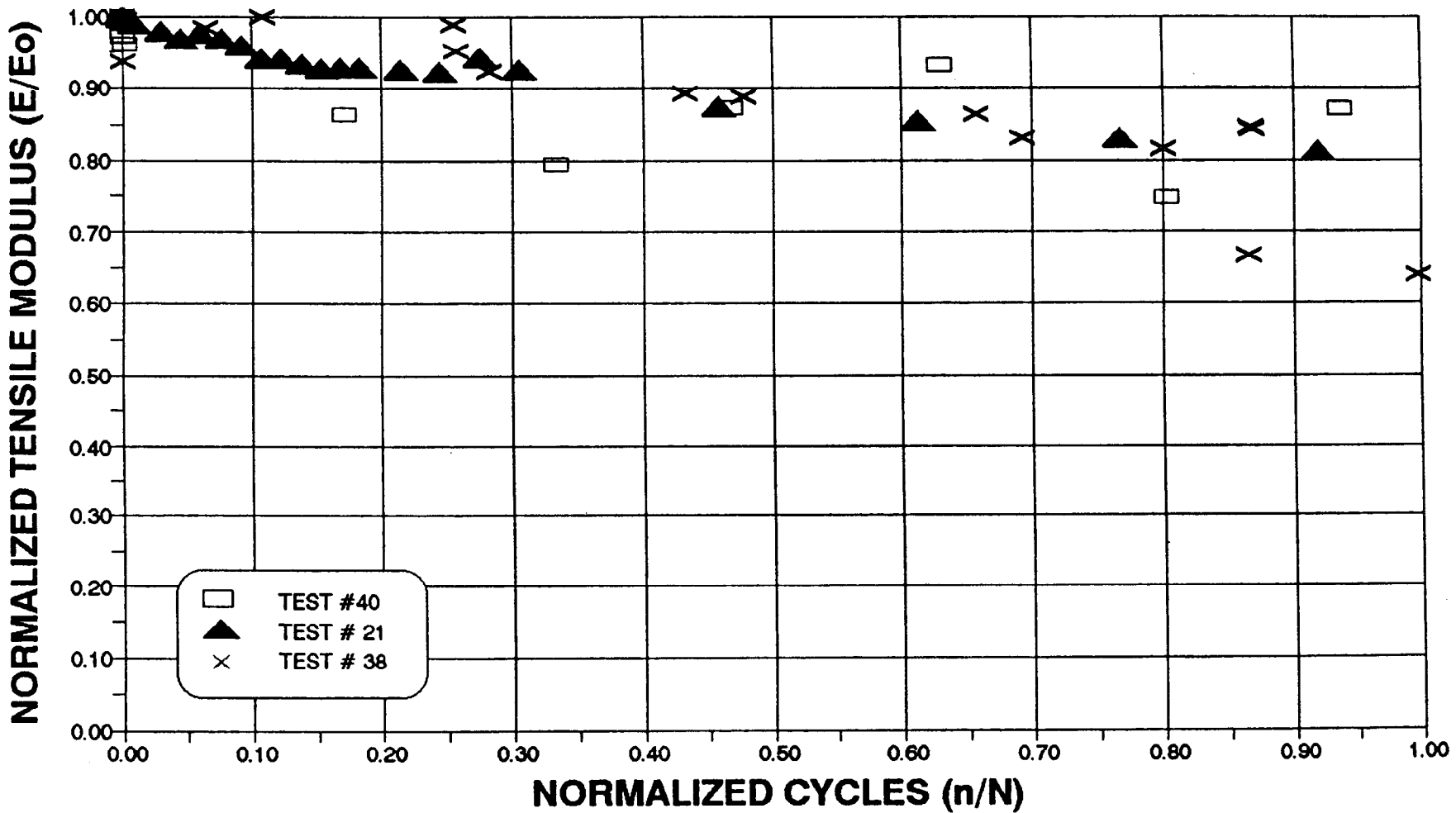


Figure 10 Modulus vs. Fractional Lifetime, Material B (Unidirectional)

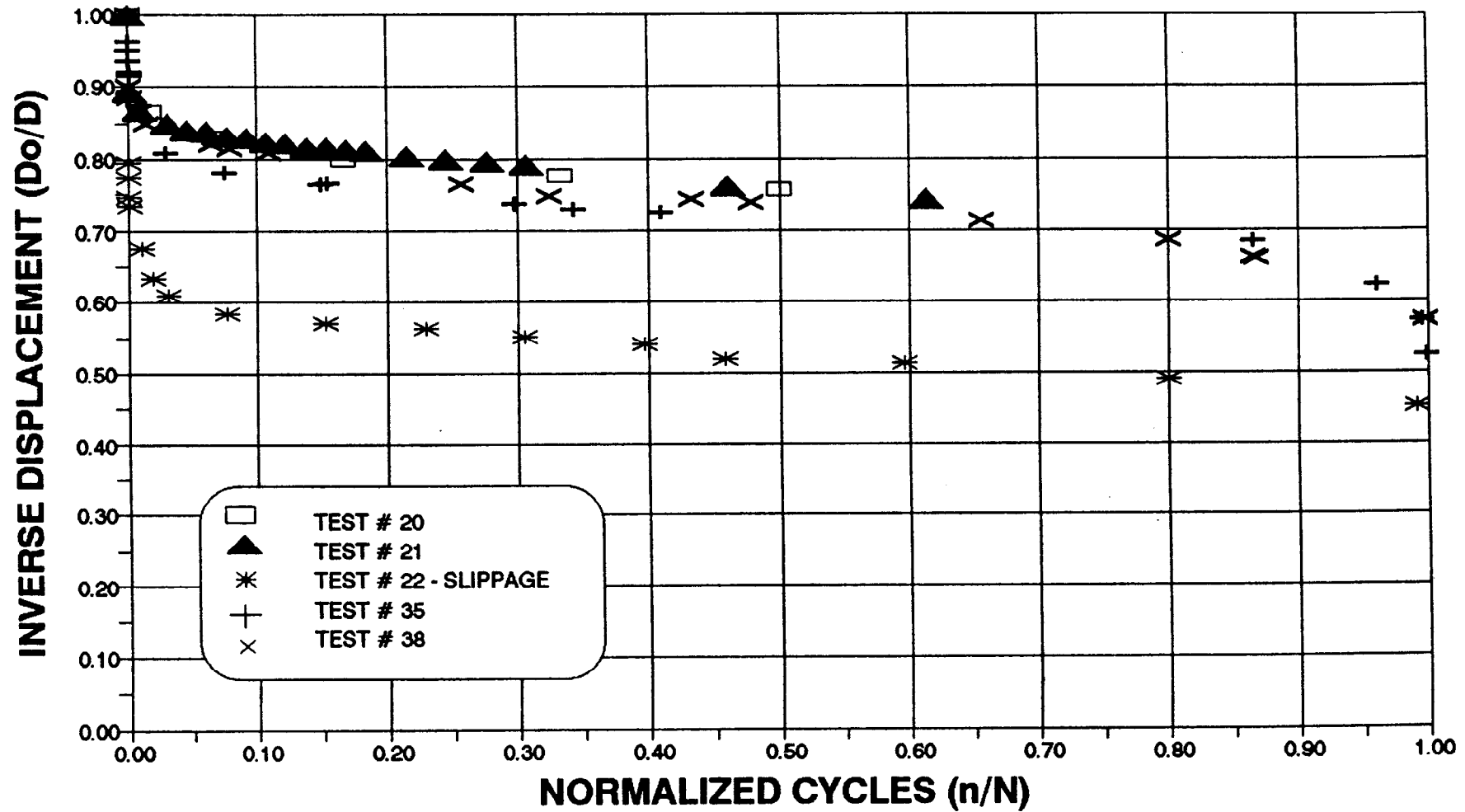


Figure 11 Normalized Inverse Displacement vs. Fractional Lifetime, Material B (Unidirectional)

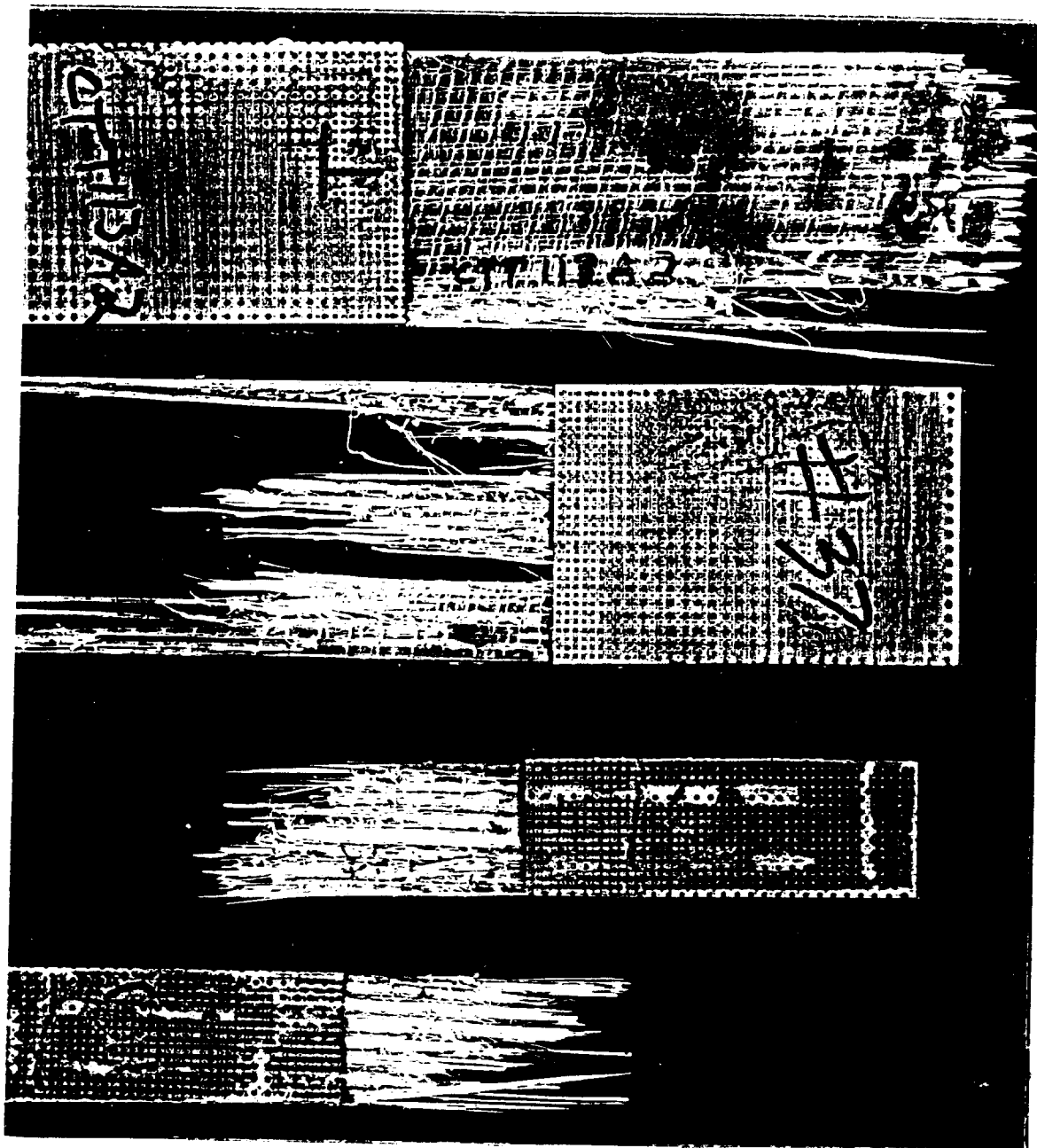


Figure 12a Typical Failures, Material A

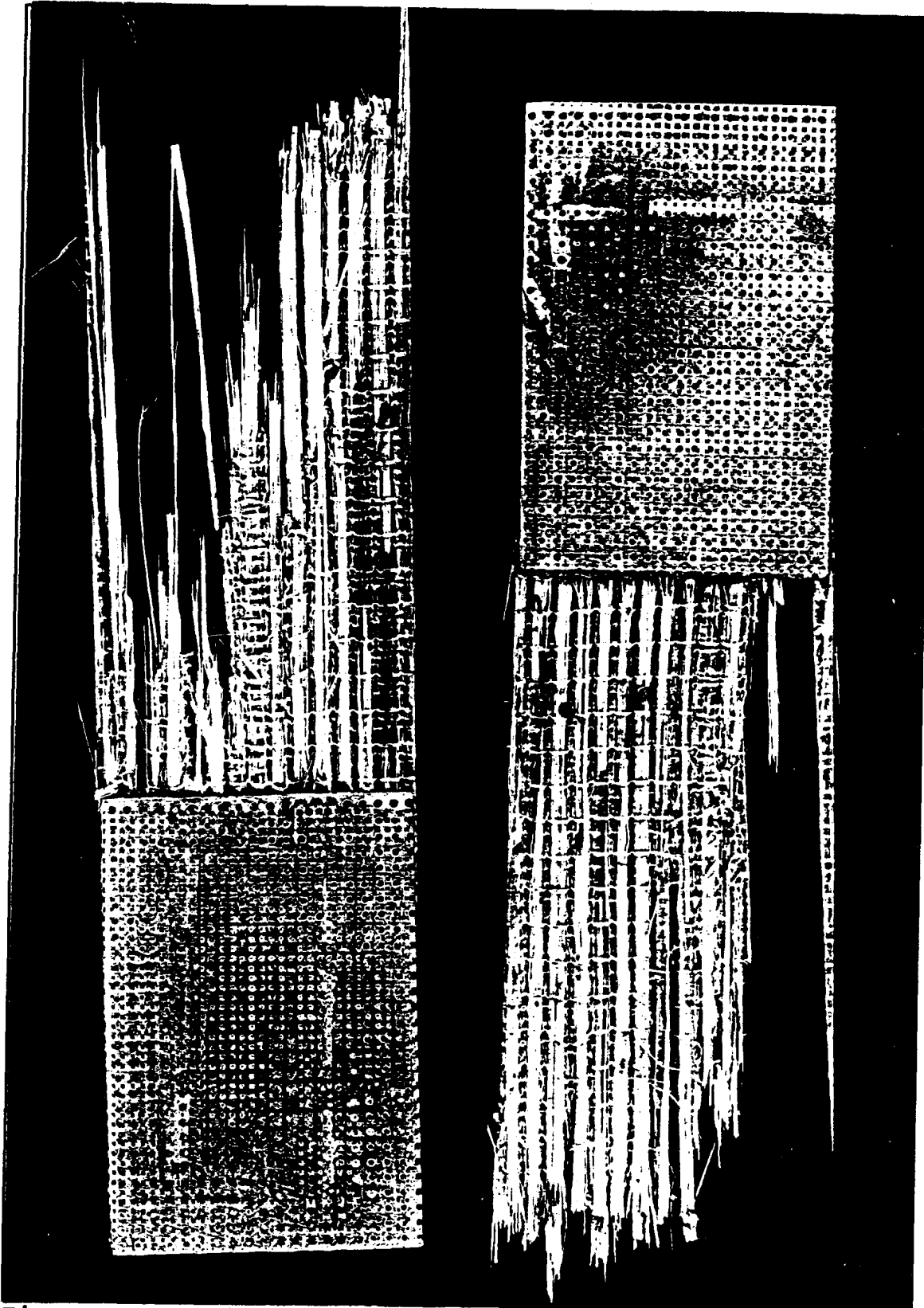


Figure 12b Typical Tab Failure of Material B Specimens.

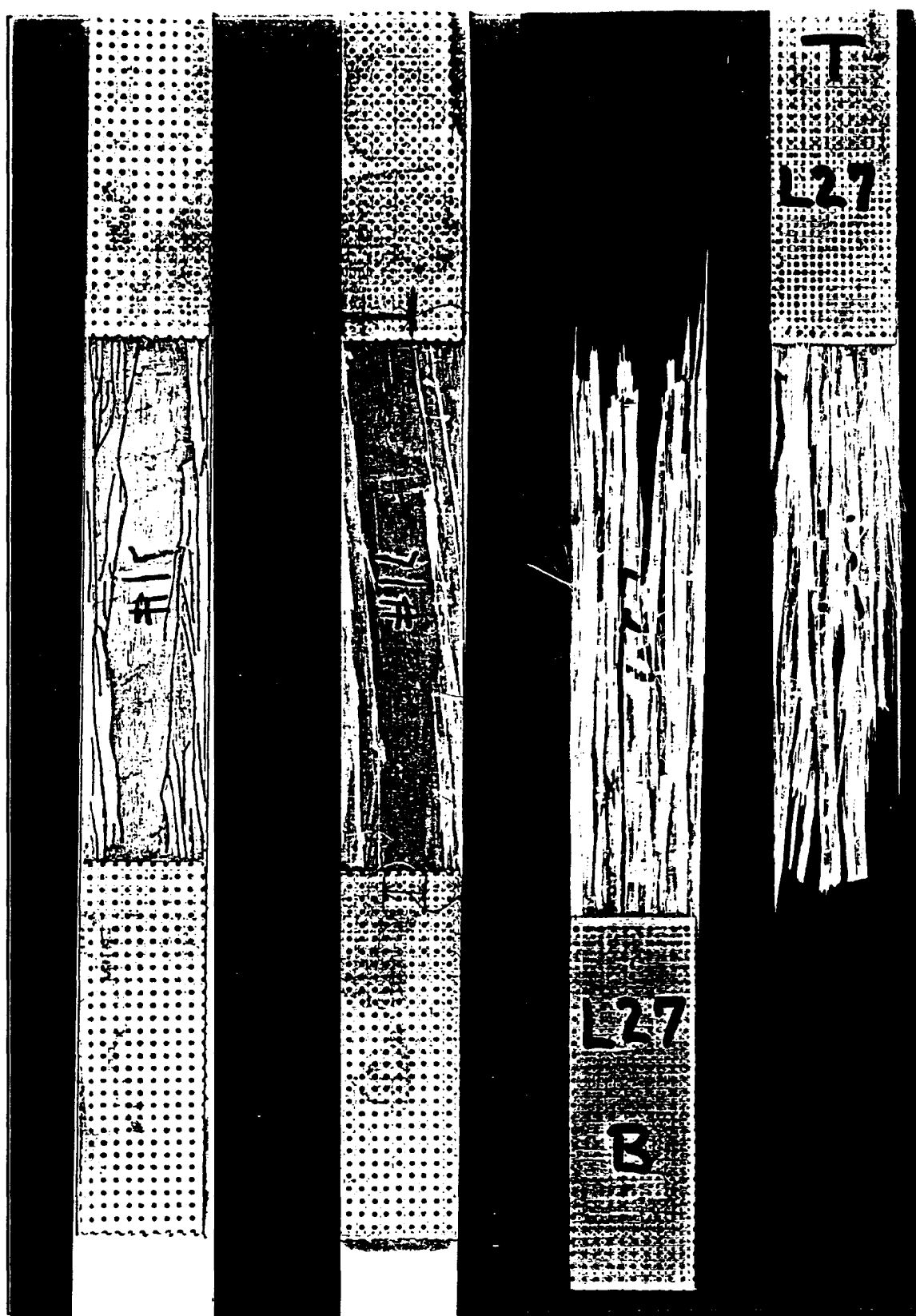


Figure 12c Typical Failures, Material C

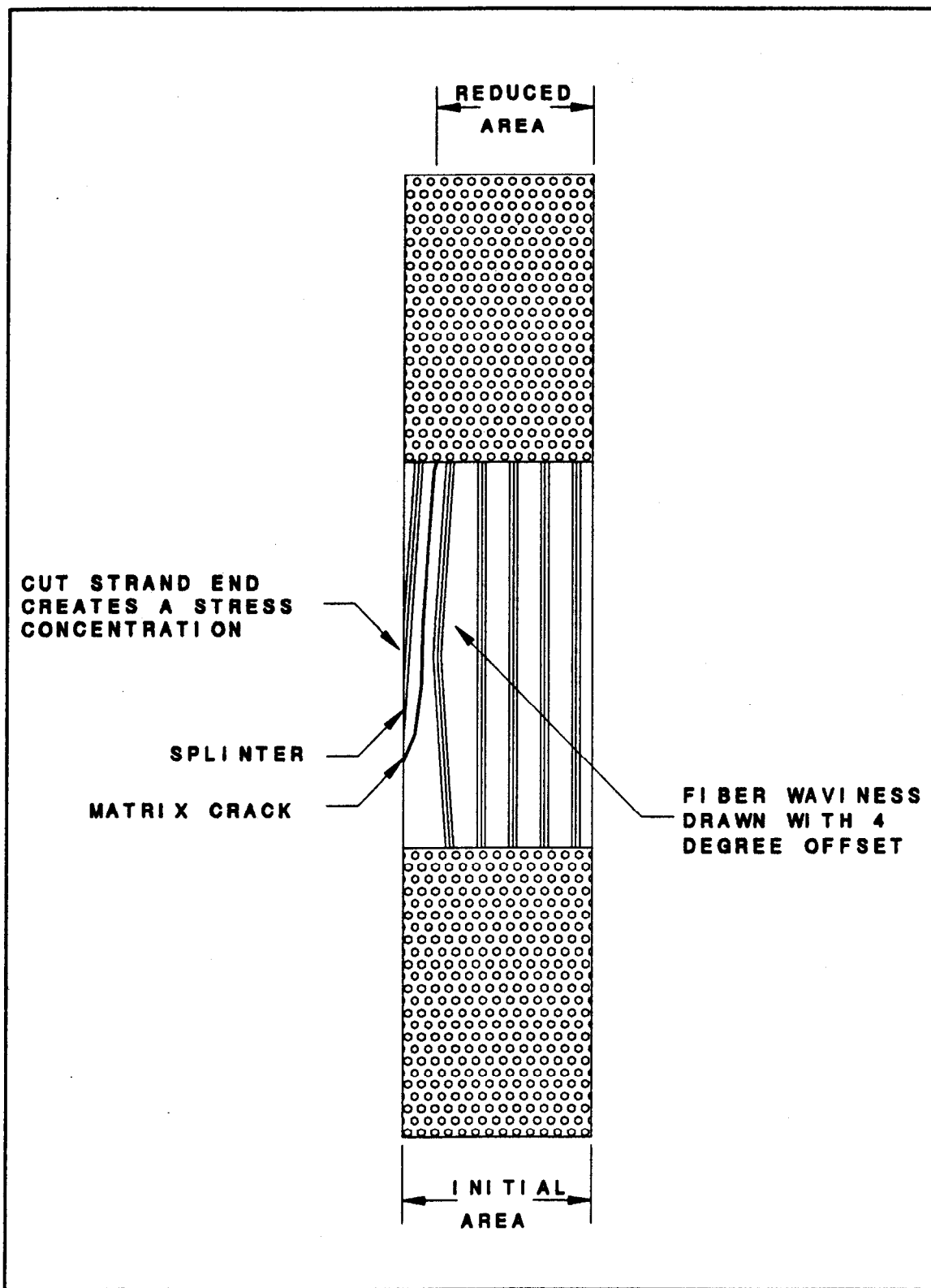


Figure 13 Schematic of Edge Splitting in Unidirectional Materials

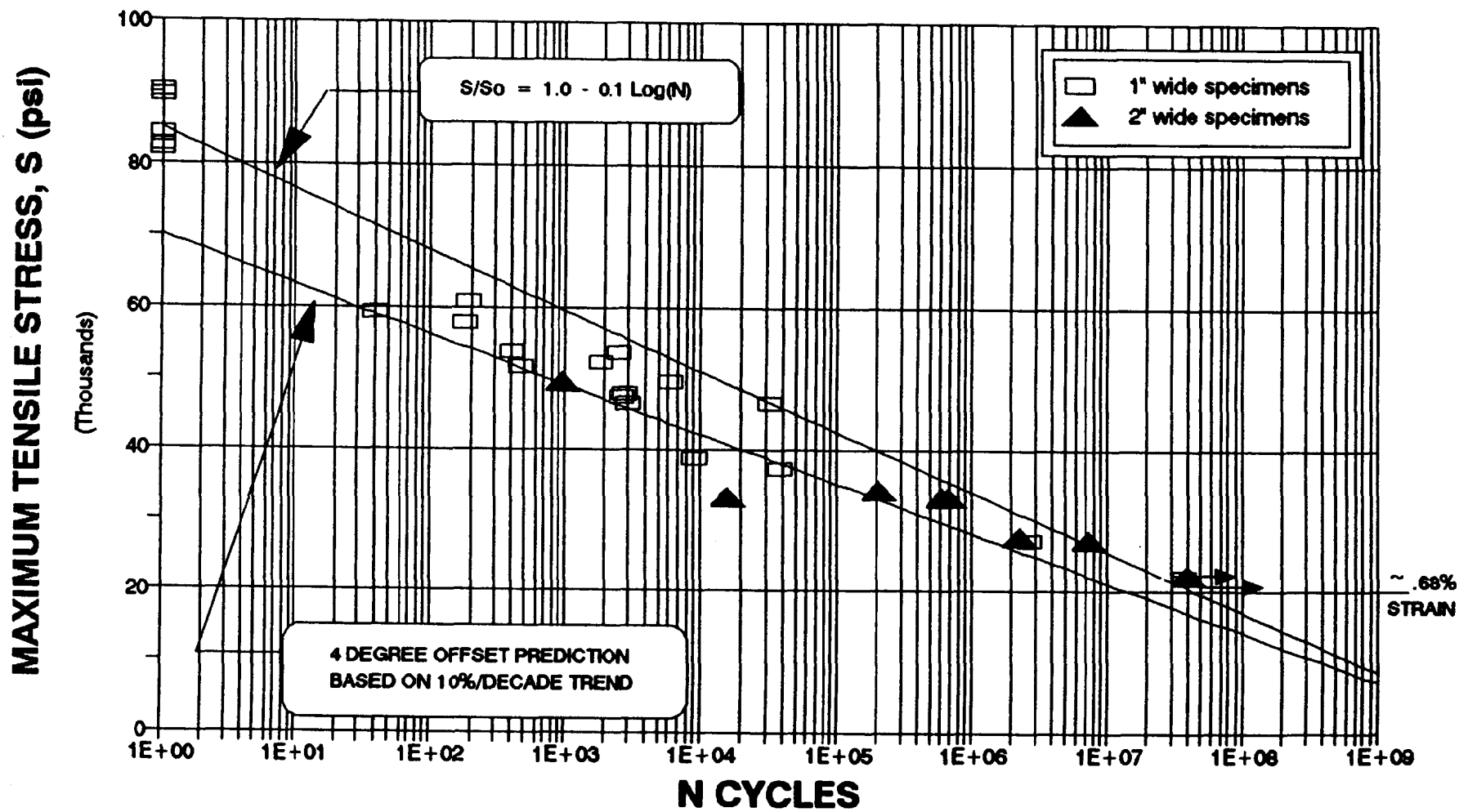


Figure 14 Material B S-N Data Fit With Eq.(1) with Cross-section Reduced to Account for 4° Edge Split

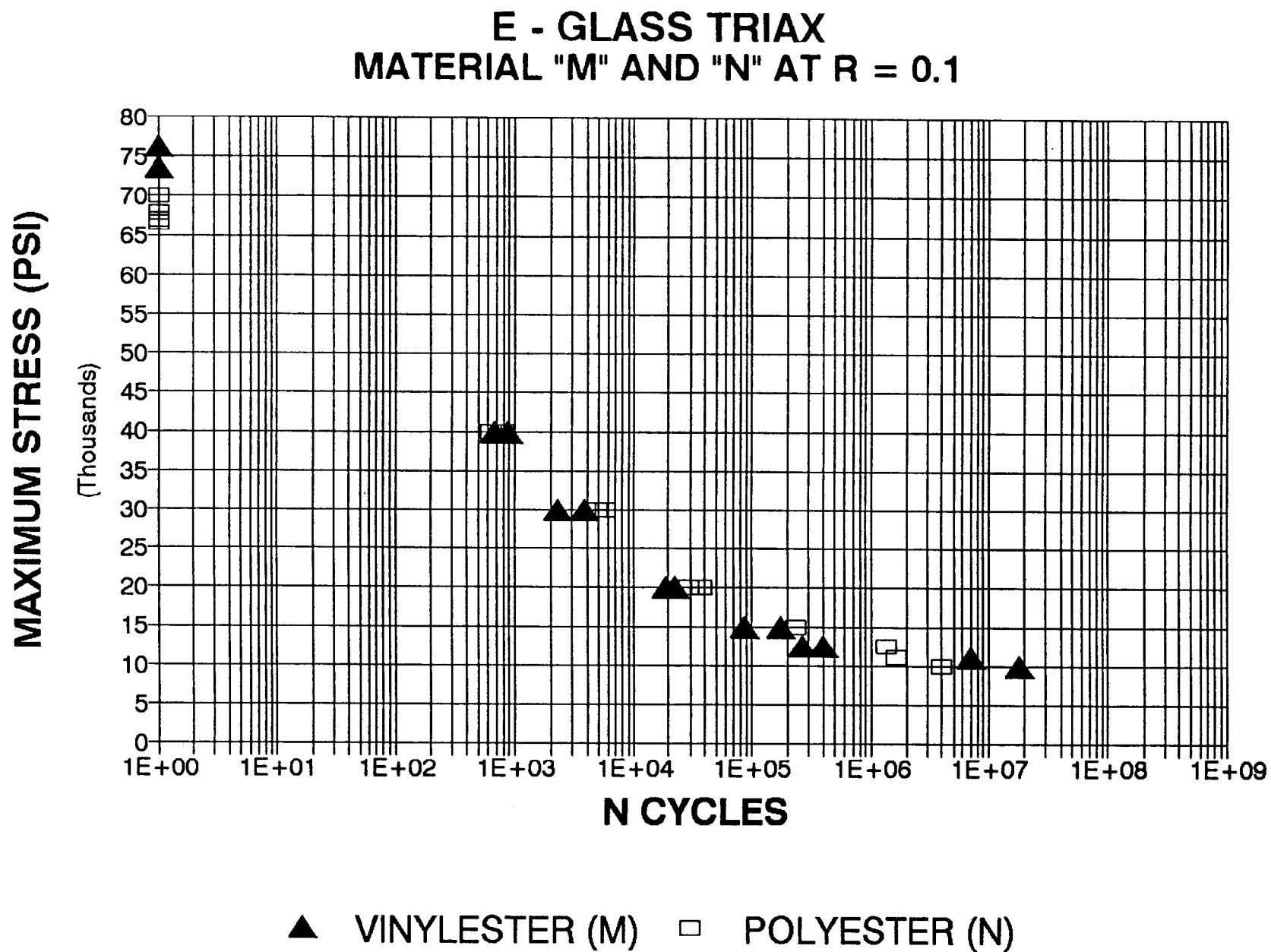


Figure 15 S-N Data for Triax Materials M (Polyester) and N (Vinylester), [0/±45]

TRIAX NORMALIZED DATA FOR MATERIALS F,G,H,J,M AND N AT R = 0.1

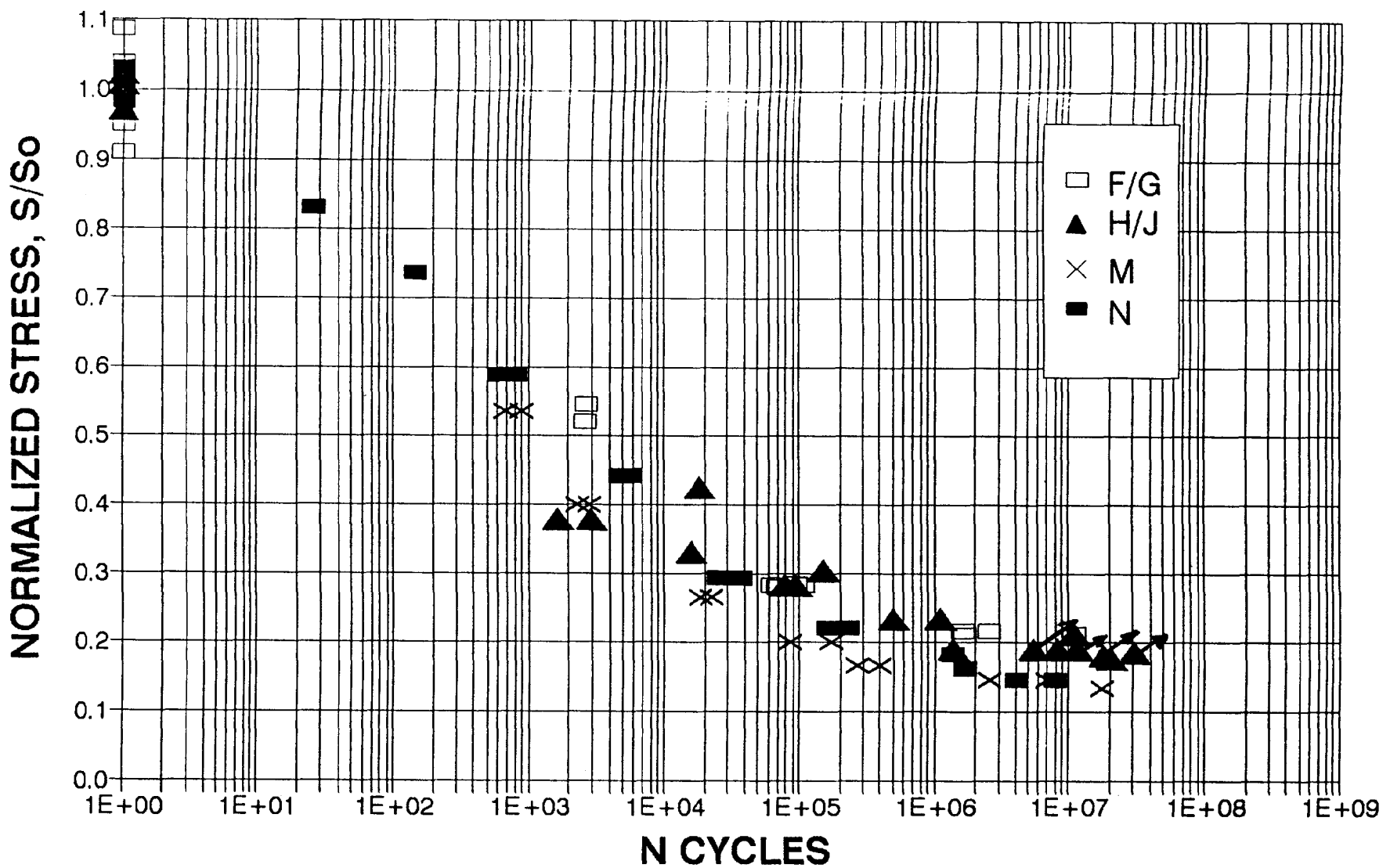


Figure 16 Normalized S-N Data for All Triax Materials

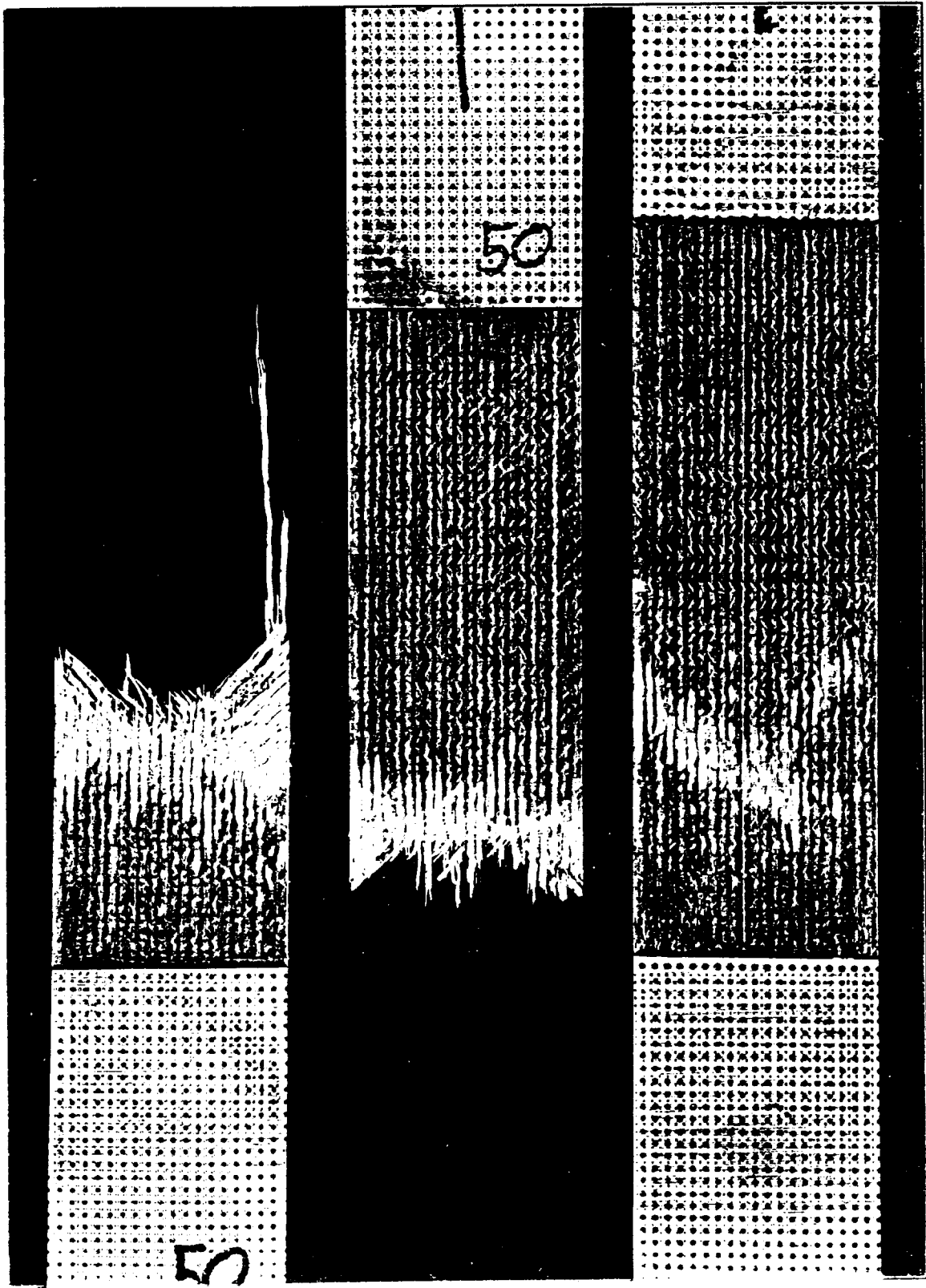


Figure 17a Damage Growth and Failure, Materials F/G

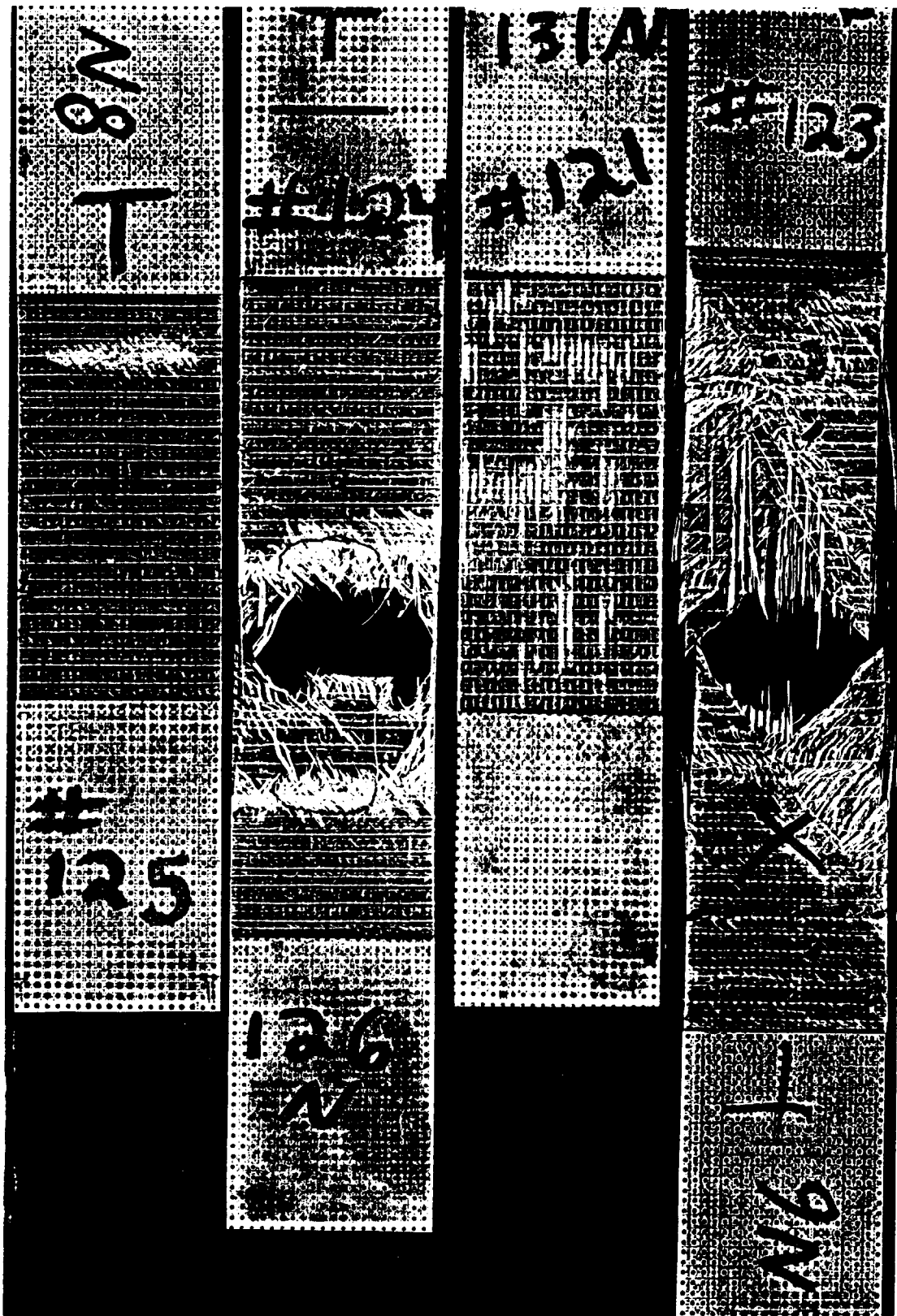


Figure 17b Typical $[0/\pm 45]$ Material N Scrim Cracking, and ± 45 Damage Region Failure Modes.

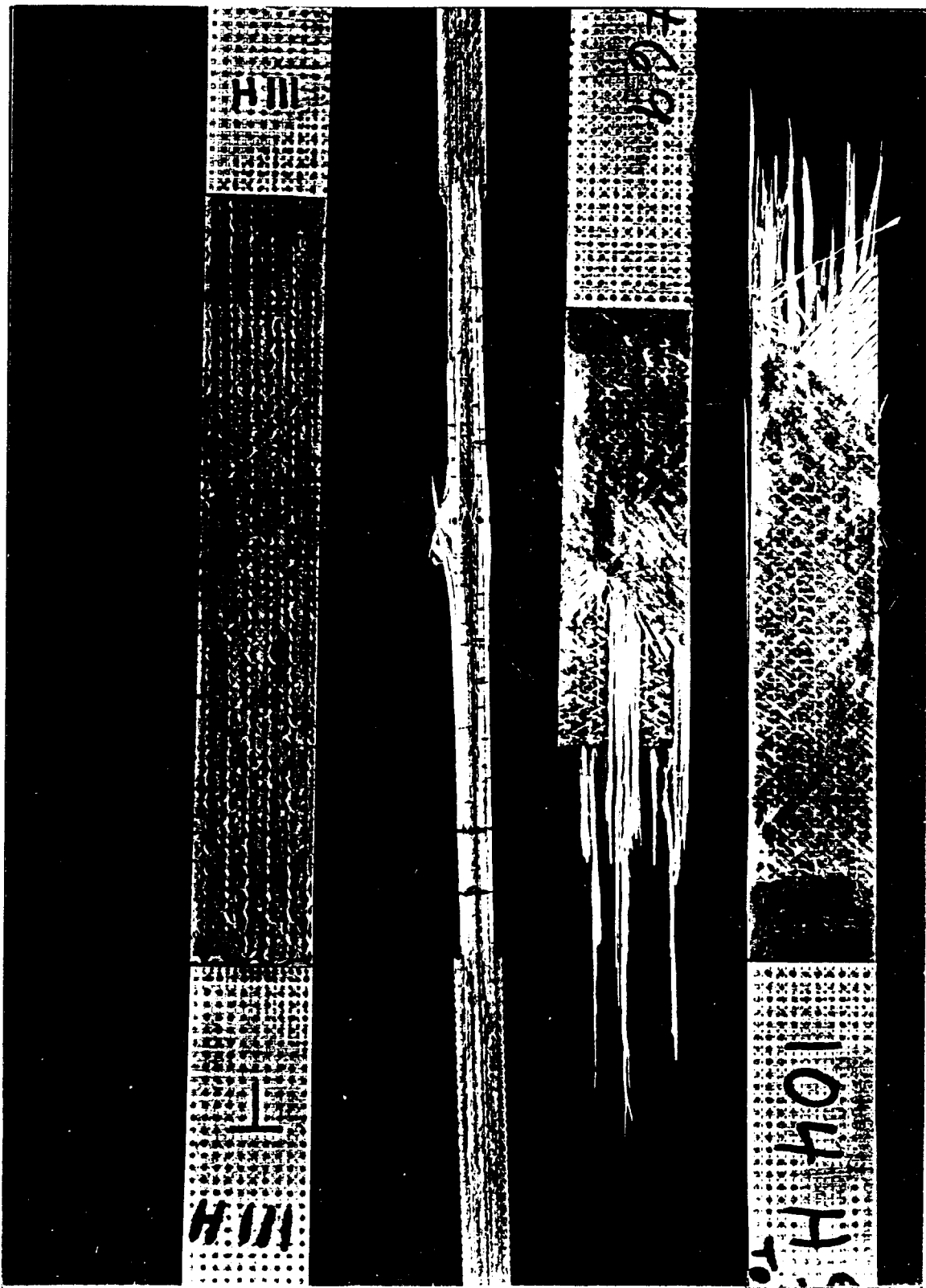


Figure 17c Materials H and J Showing Matrix Cracking and Failure

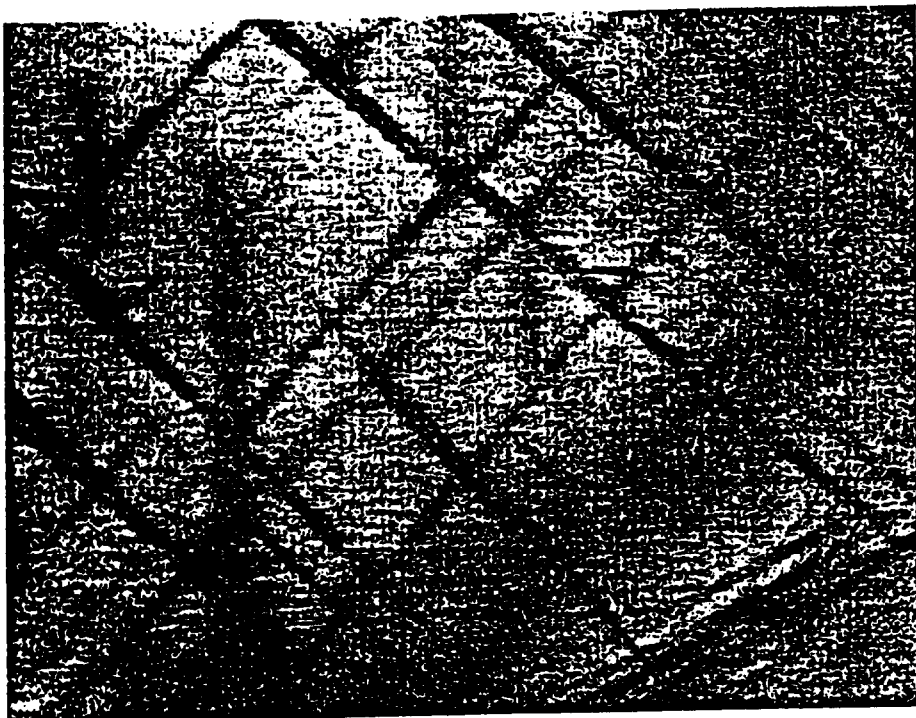


Figure 18 Cracking of 45° Plies in Material N

fractured

relative size only

Figure 19 Cracking Zone in Material N

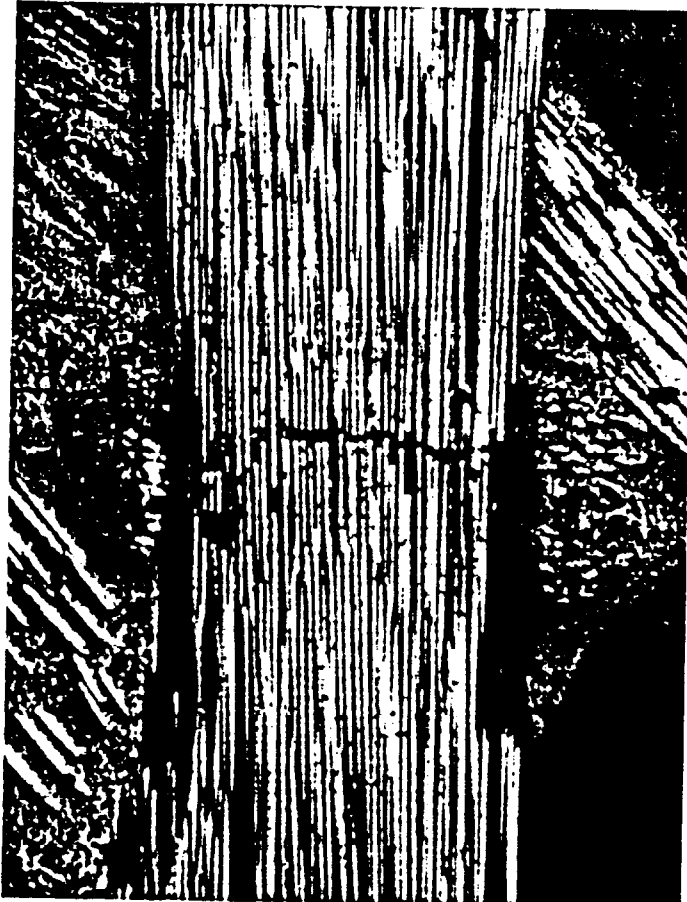


Figure 20 Failure of 0° Strand in a Cracking Zone, Material N

INITIAL STRAIN LEVEL VS. CYCLES UNIDIRECTIONAL AND TRIAXIAL MATERIALS

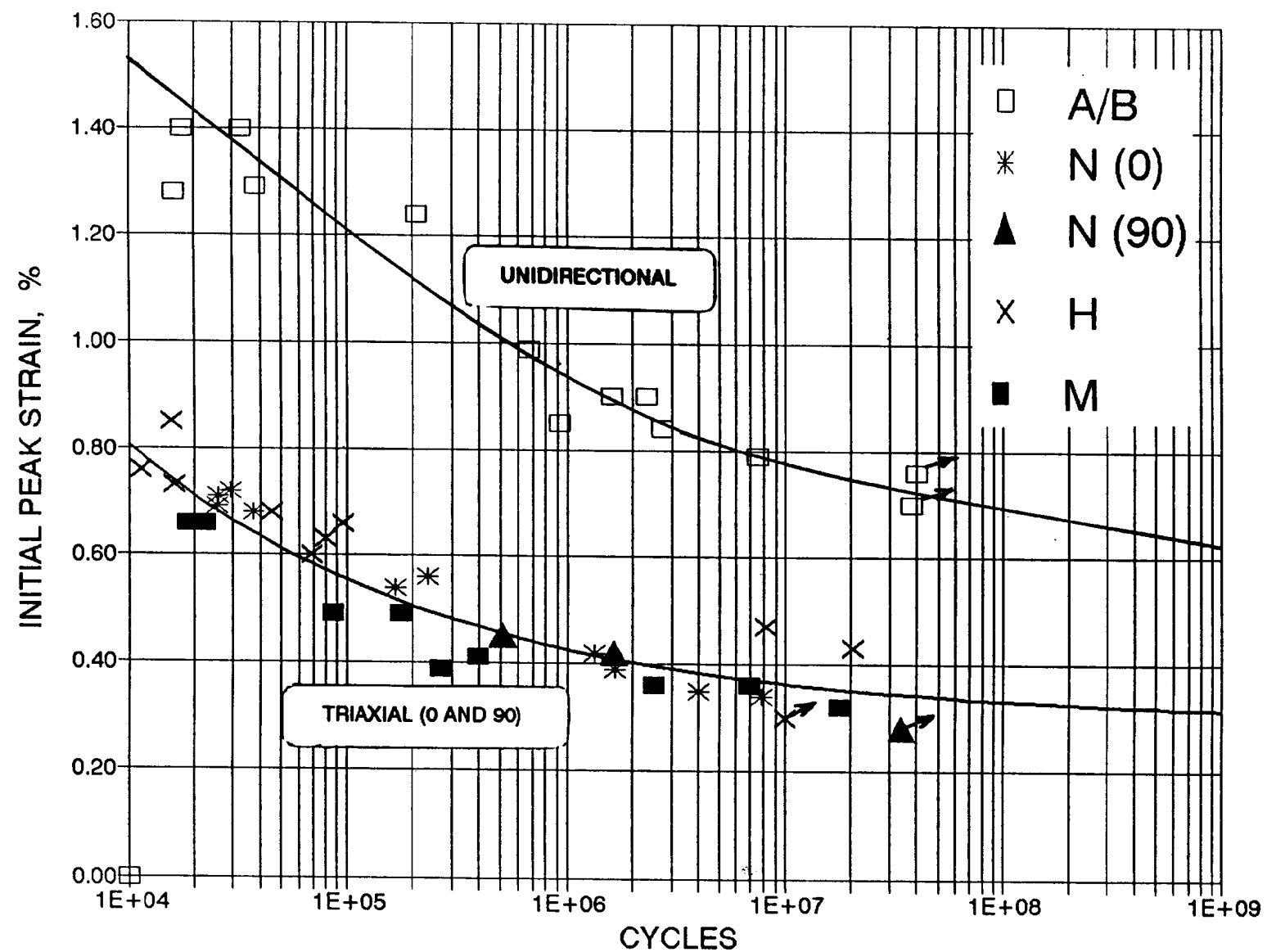


Figure 21 Initial Strain vs. Cycles to Failure, Unidirectional and Triaxial Materials

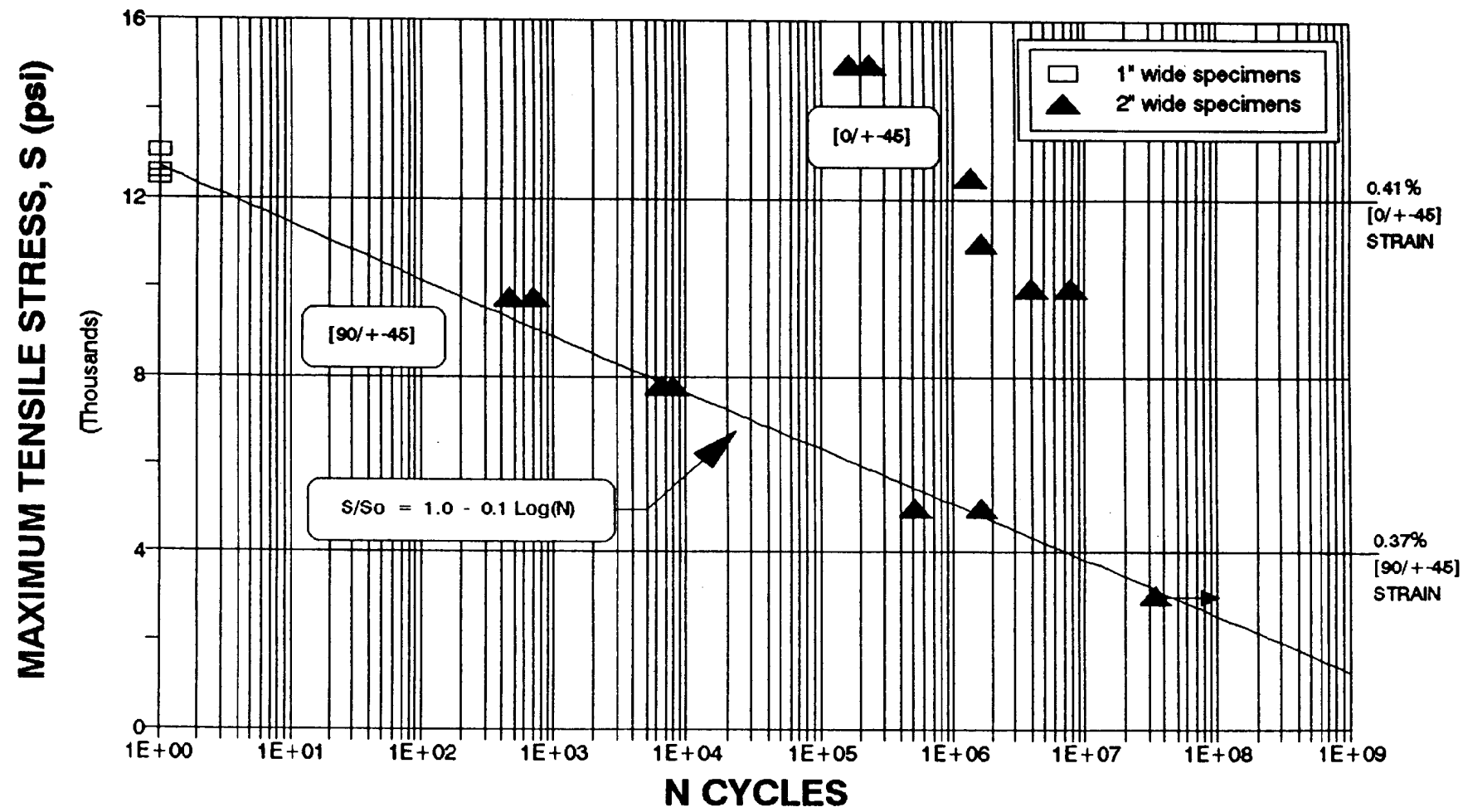


Figure 22 S-N Data for Material N Tested Transversely, [90/ \pm 45] vs. [0/ \pm 45]

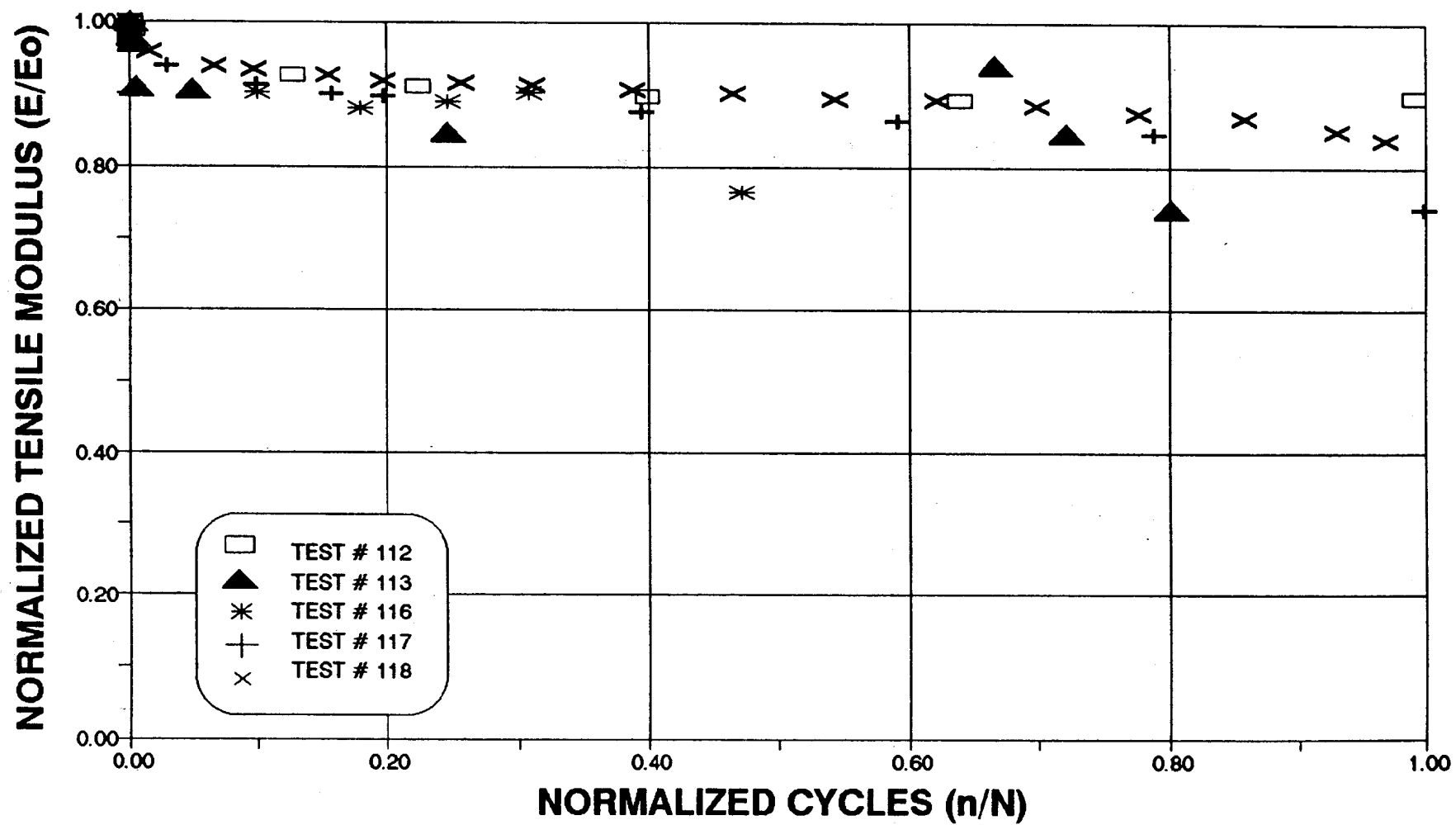


Figure 23 Modulus vs. Fractional Lifetime, Material N Tested as [0/±45]

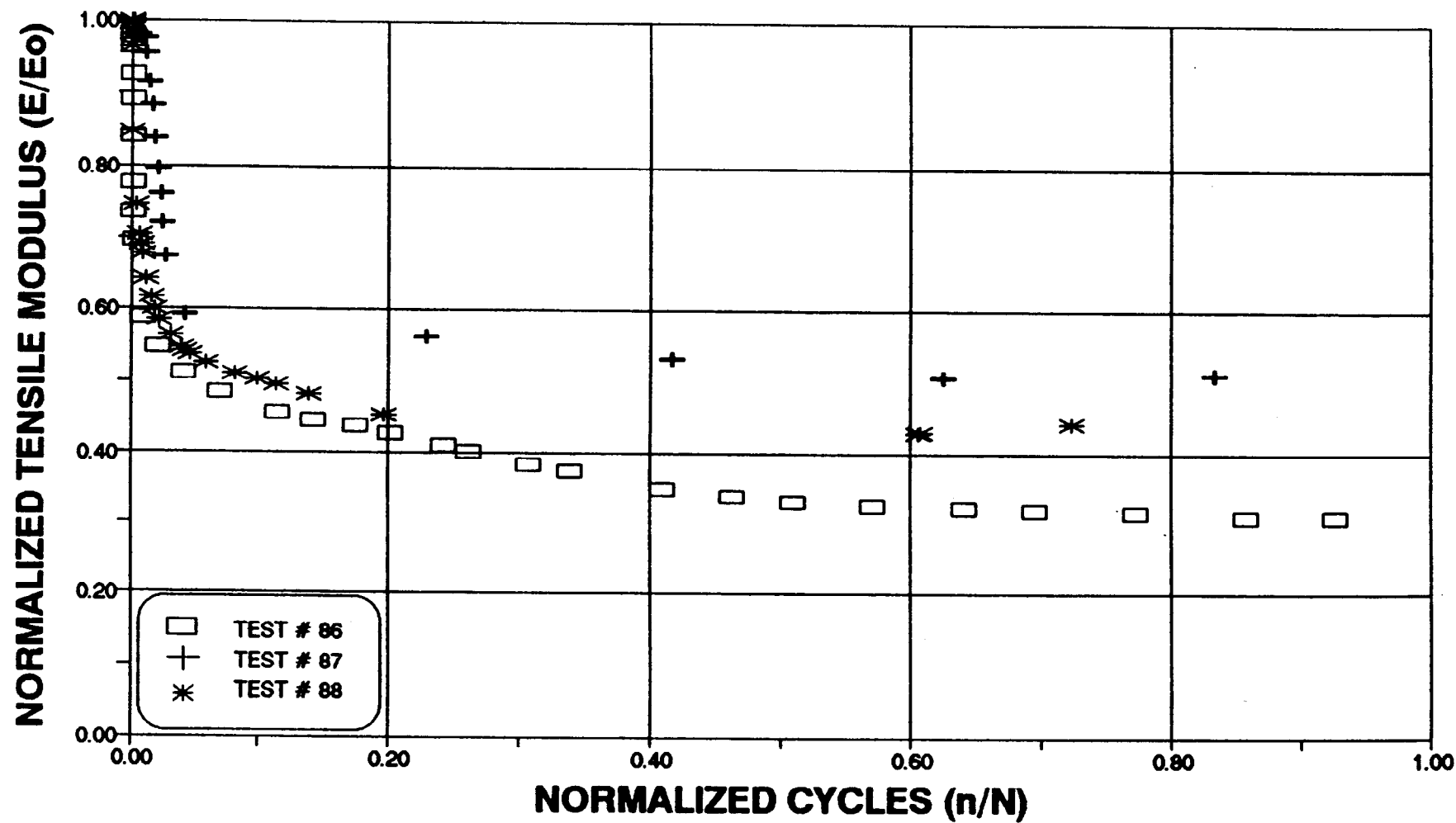


Figure 24 Modulus vs. Fractional Lifetime, Material N Tested Transversely [90/ ± 45]

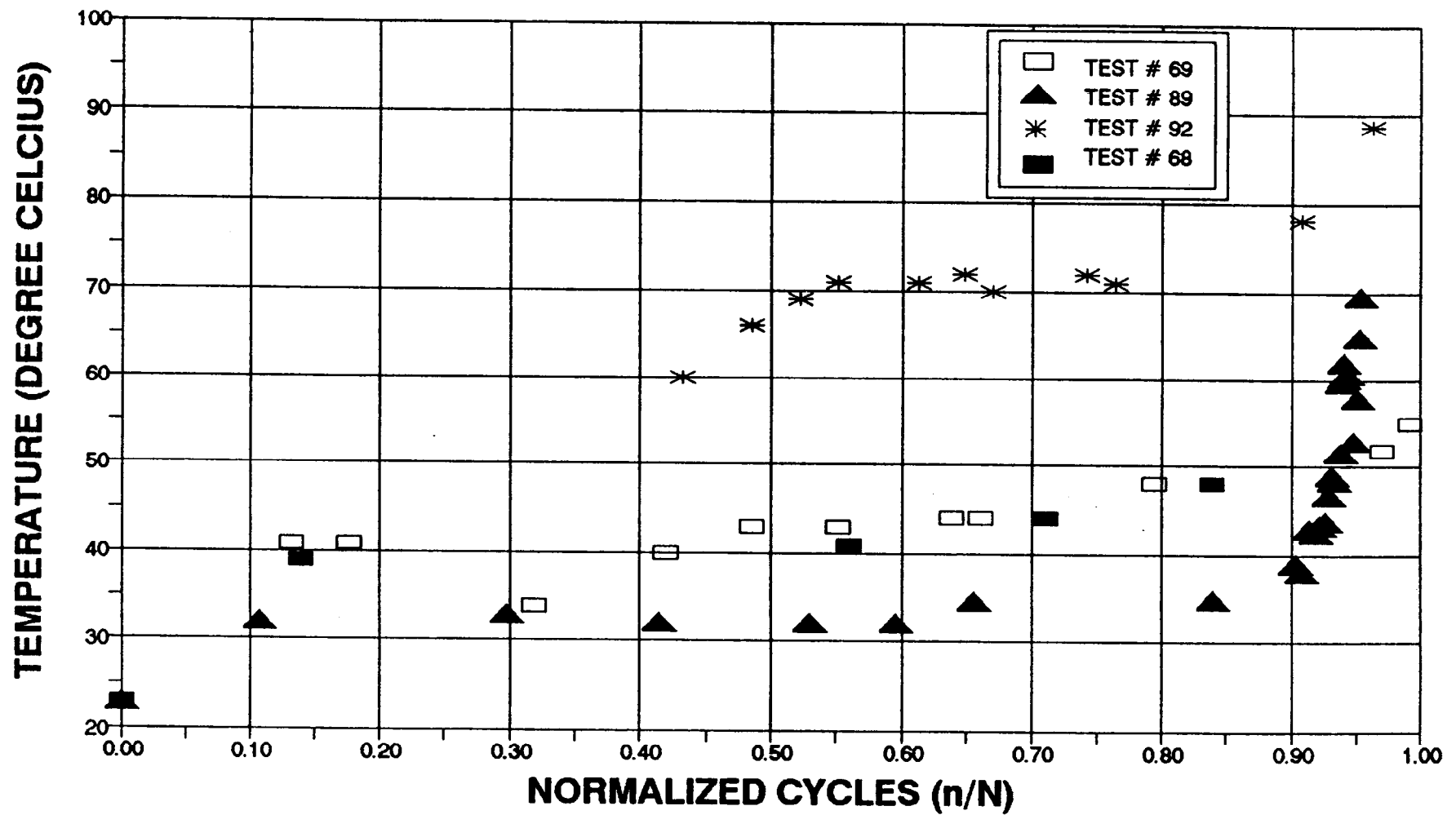


Figure 25 Surface Temperature vs. Fractional Lifetime, Materials H and J with Joint

48

TRIAx FATIGUE DATA MATERIALS H AND J AT R = 0.1

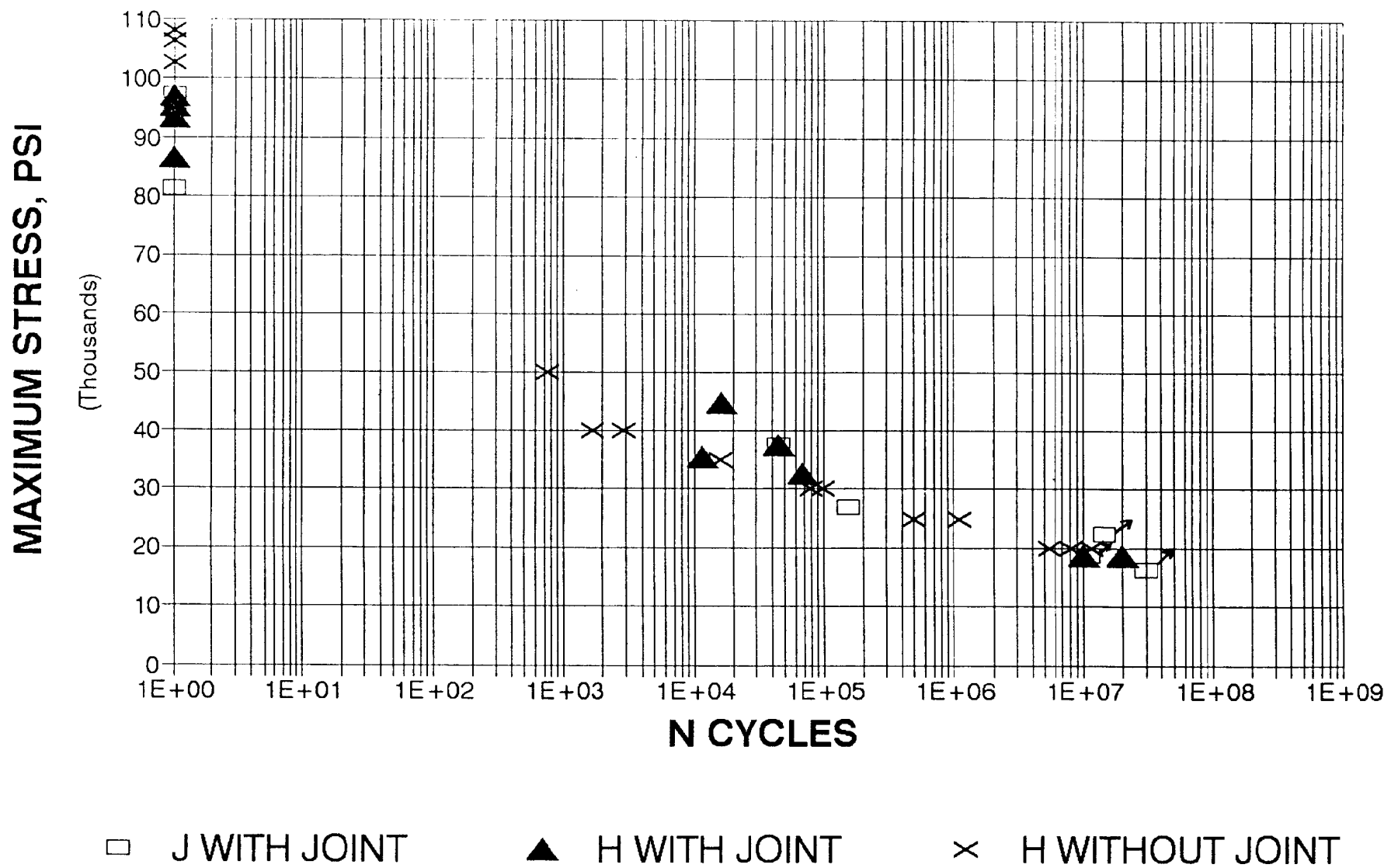


Figure 26 S-N Data for Materials H and J with and without Joint in Gage Section (Stress Based on Net Cross-Section)

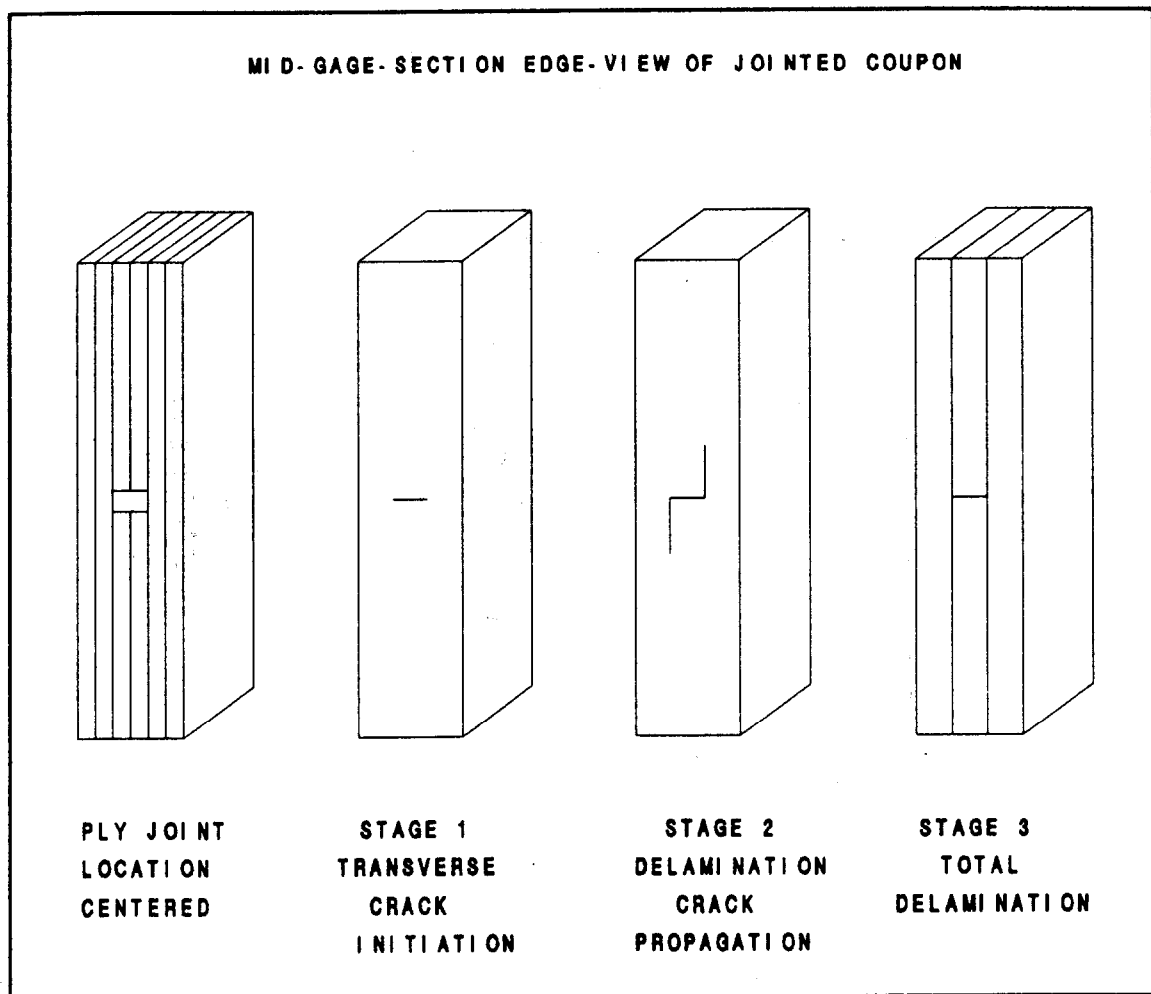


Figure 27 Schematic of Delaminations in Materials H/J

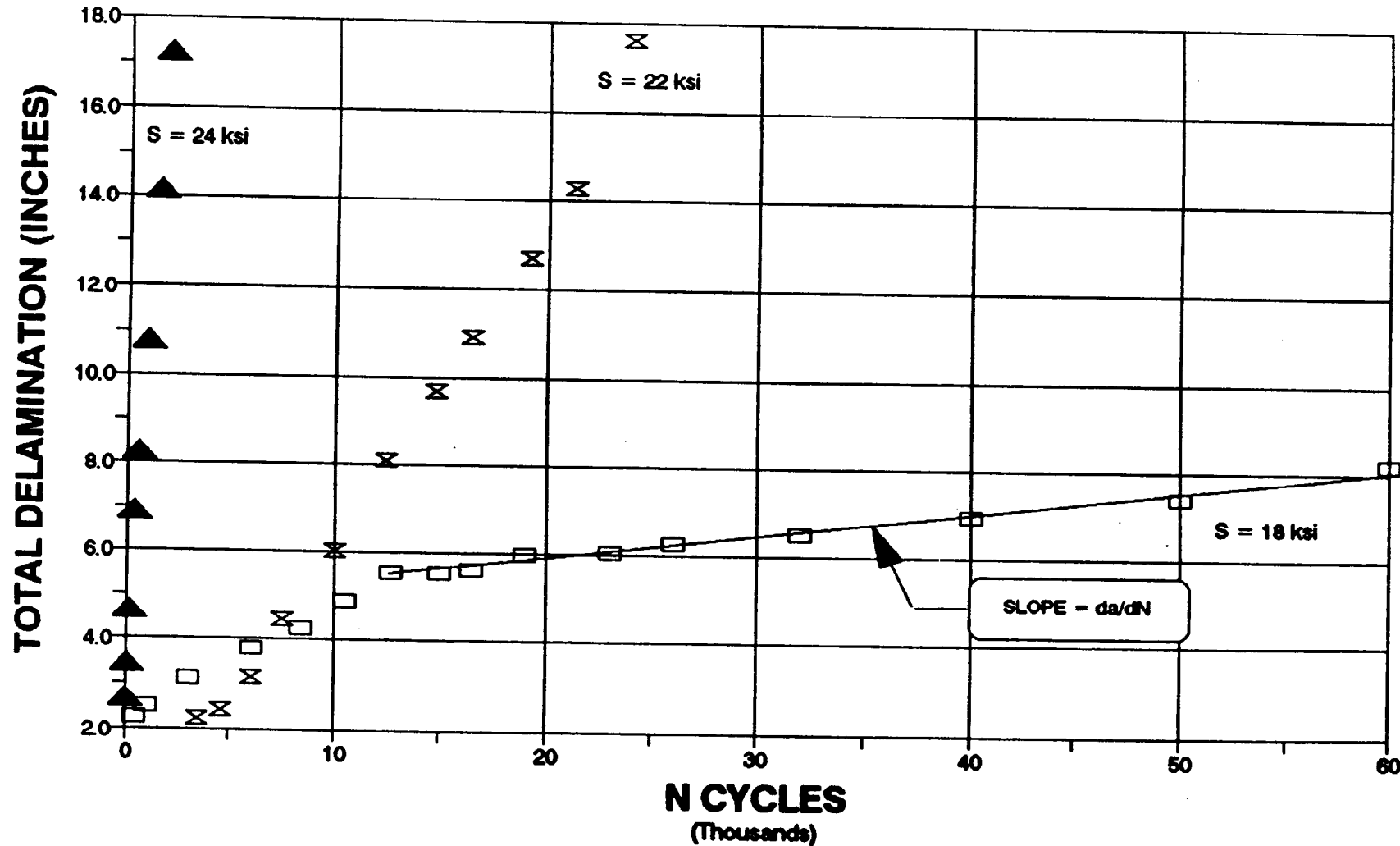


Figure 28 Typical Data for Delamination Total Length vs. Cycles at Three Stress Levels, Materials H/J

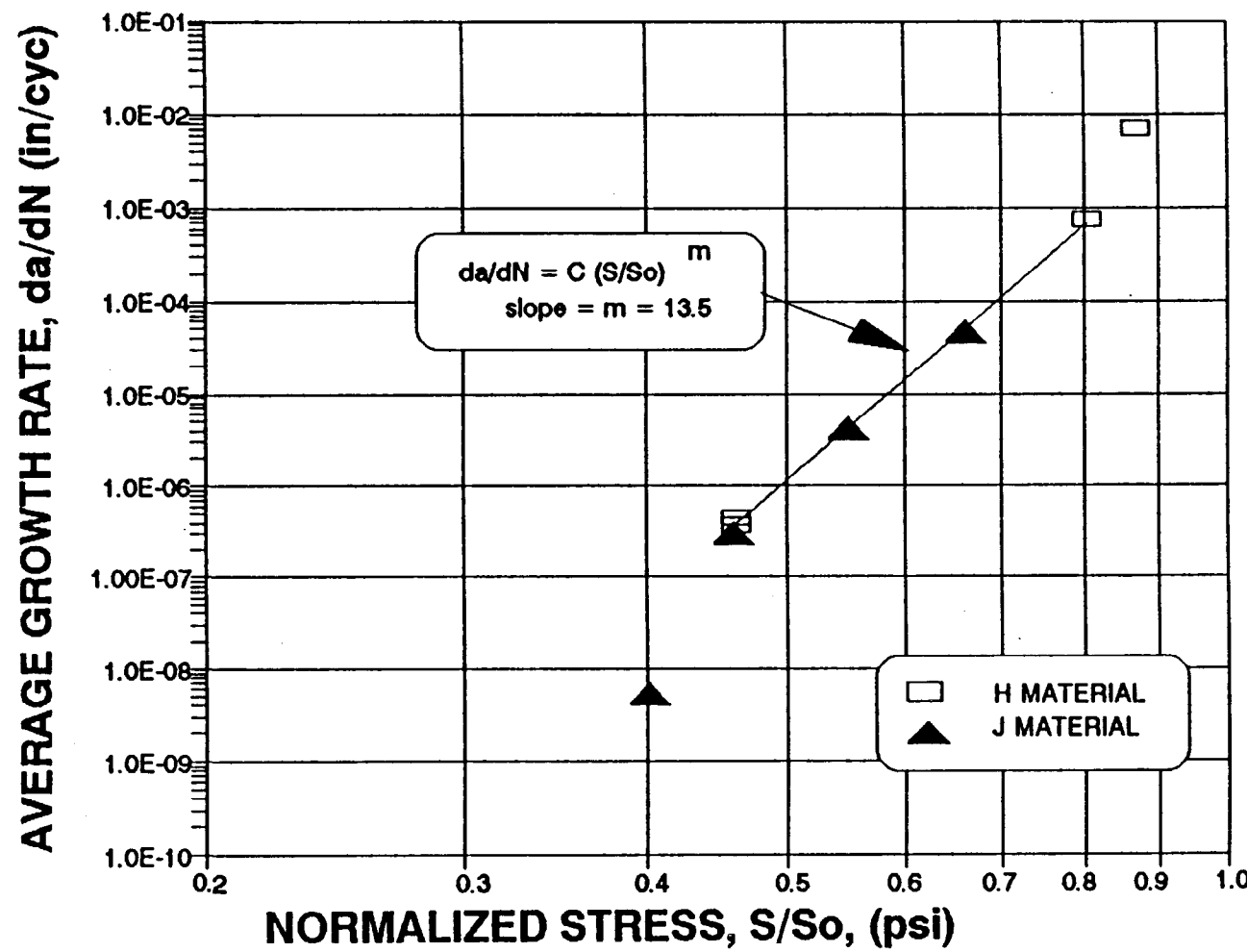


Figure 29 Delamination Crack Growth Rate Data for Materials H/J vs. Normalized Stress ($S_0 = 27$ ksi)

APPENDIX

This Appendix lists the results of all static and fatigue tests in alphabetical order of the material tested. The following should be noted regarding the data column headings, from left to right.

1. The test number identifies the test and specimen in the overall program.
2. The Specimen number identifies the particular specimen for a given material system. The letter is the material designation used at MSU, not the original designation of the supplier.
3. The stress given is the maximum stress in the constant stress amplitude fatigue tests, or the maximum stress reached in a single cycle (ramp) static test.
4. R is the stress ratio = minimum stress/maximum stress; * indicates a static test.
5. Q is the frequency of fatigue tests in Hertz (cycles/second), or the ramp rate in static tests in inches/second (constant stroke rate).
6. E is the Young's modulus in the load direction, measured in a preliminary test at low stress, prior to fatigue tests.
7. e is the maximum strain (in %) on the initial cycle or first few cycles of fatigue tests; for static tests e is the strain at failure.
8. The cycles to total separation, N, are given in column 8 unless otherwise noted in column 9.
9. The specimen nominal width (first number, in inches) failure type and location, and other information given in column 10 identified on the last page.

SUMMARY OF FIBERGLASS FATIGUE RESULTS MATERIAL A

TEST & SAMPLE ID #	STRESS PSI	R	Q Hz	E MSI	e %	CYCLES TO FAIL	FAILURE MODE
23 111A	40480/4048	0.1	5	2.90	1.4	17700	2LTC
25 112A	30800/3080	0.1	10	3.24	----	138596	2UTC
30 121A	85670	*	0.5	3.25	2.83	1	1MGB
31 120A	82170	*	0.5	2.89	2.82	1	1MGB
32 119A	78945	*	0.5	2.96	2.64	1	1MGB
36 114A	27430/2743	0.1	10	3.04	0.90	1612585	2UTSC
37 113A	27785/2779	0.1	10	3.28	0.85	920132	2UTJ
97 137A	79500	*	0.25	3.19	2.20	1	1MGB
98 136A	84040	*	0.25	3.36	2.30	1	1MGB
180 138A	-46843	*	0.25	----	----	1	1MGE
181 139A	-46198	*	0.25	----	----	1	1MGE
182 140A	-43242	*	0.25	----	----	1	1MGE

SUMMARY OF FIBERGLASS FATIGUE RESULTS MATERIAL B

TEST & SAMPLE ID #	STRESS PSI	R	Q Hz	E MSI	e %	CYCLES TO FAIL	FAILURE MODE
9 103B	53600/5360	0.1	1	----	----	2584	1LTSJ
12 108B	38700/3870	0.1	5	----	----	9173	1LTSC
13 109B	47500/4750	0.1	5	3.03	1.8	2640	1LTSJ
15 111B	56130/5613	0.1	0.1	2.69	2	7	1LGB
16 112B	37200/3720	0.1	5	2.92	1.29	38133	1LTJ
17 113B	48100/4810	0.1	5	3.11	1.53	2841	1LTJ
18 114B	53900/5390	0.1	1	2.83	1.90	415	1LGJ
20 116B	46600/4660	0.1	5	2.79	1.6	3008	1LTSJ
21 107B	46500/4650	0.1	4	3.28	1.4	32640	1LTC
22 117B	33200/3320	0.1	10	----	----	655147	2LTSJ
24 118B	49700/4970	0.1	1	2.34	1.9	981	2UTJ
26 119B	82800	*	0.5	3.23	2.36	1	1UGJ
27 123B	90200	*	0.5	3.11	2.73	1	1GBJ
28 124B	82800	*	0.5	3.07	2.76	1	1UTJ
29 125B	84500	*	0.5	3.31	2.77	1	1UGJ
33 120B	33200/3320	0.1	10	3.08	1.08	16156	2LTC
34 121B	34400/3440	0.1	5	2.78	1.24	206864	2UTC
35 122B	33200/3320	0.1	10	3.35	0.99	671333	2ULTJ
38 126B	27585/2759	0.1	10	3.01	0.90	2310849	2UTSC
39 129B	22290/2229	0.1	15	2.89	0.76	40000000	2RO
40 130B	27250/2725	0.1	10	3.27	0.79	7475243	2LTSC
56 135B	27130/2713	0.1	10	3.24	0.84	2720584	1UTC
57 133B	21985/2199	0.1	15	3.15	0.70	37906456	1RO
58 127B	89730	*	1.0	3.25	2.90	1	1MGJ
61 137B	82330	*	1.0	2.95	2.79	1	1MGB
64 138B	35503	*	1.0	----	----	1	1MGDB
66 138B	49700/4970	0.1	1	3.03	1.64	6085	1UGJ
99 128B	81150	*	0.25	2.88	2.82	1	1MGJB
100 131B	81085	*	0.25	3.54	2.29	1	1MGJB
183 139B	-38405	*	0.25	----	----	1	2MGE
184 140B	-40988	*	0.25	----	----	1	2MGE
185 141B	-40297	*	0.25	----	----	1	2MGE

186	142B	-43922	*	0.25	----	----	1	2MGE
187	143B	-44545	*	0.25	----	----	1	2MGE

SUMMARY OF FIBERGLASS FATIGUE RESULTS MATERIAL F

TEST & SAMPLE ID #	STRESS PSI	R	Q Hz	E MSI	e %	CYCLES TO FAIL	FAILURE MODE
41 105F	53700	*	0.5	2.58	2.08	1	1MGDBY
44 106F	52600	*	0.5	2.12	3.55	1	1MGDBY
45 108F	49130	*	0.5	2.78	1.77	1	1MGDBY
47 109F	28225/2823	0.1	5	----	----	2689	1MGDBY
49 101F	14830/1483	0.1	5	----	----	95101	2LGDBY
51 104F	11250/1125	0.1	10	----	----	1615838	2LGAY
53 103F	11250/1125	0.1	10	----	----	2487507	2MGCY
55 111F	14750/1475	0.1	10	----	----	108029	1UGCN
188 119F	-54129	*	0.25	----	----	1	2MGEN
189 120F	-52740	*	0.25	----	----	1	2MGEN
190 121F	-49359	*	0.25	----	----	1	2MGEN
191 122F	-54846	*	0.25	----	----	1	2MGEN

SUMMARY OF FIBERGLASS FATIGUE RESULTS MATERIAL G

TEST & SAMPLE ID #	STRESS PSI	R	Q Hz	E MSI	e %	CYCLES TO FAIL	FAILURE MODE
42 105G	57530	*	0.5	2.31	2.49	1	1MGDBY
43 106G	53095	*	0.5	2.38	3.51	1	1MGDBY
46 108G	48180	*	1.0	----	----	1	1MGDBY
48 107G	27550/2750	0.1	5	----	----	2637	1LGDBY
50 101G	14900/1490	0.1	10	----	----	69052	2LGDBY
52 102G	11155/1116	0.1	10	----	----	1669945	2LGAY
54 109G	14970/1497	0.1	10	----	----	65372	1LGCN
67 110G	11250/1125	0.1	10	2.58	0.43	11160358	1LGJN
107 104G	51070	*	0.25	2.85	1.79	1	1MGBY
108 105G	51850	*	0.25	2.96	1.75	1	1MGBY

SUMMARY OF FIBERGLASS FATIGUE RESULTS MATERIAL H

TEST & SAMPLE ID #	STRESS PSI	R	Q Hz	E MSI	e %	CYCLES TO FAIL	FAILURE MODE
59 101H	62218	*	1.0	3.74	3.24	1	1MGDBY
60 102H	57680	*	1.0	2.72	2.12	1	1MGDBY
69 104H	25015/2502	0.1	5	3.65	0.68	45360	1LGJY
71 106H	70370	*	0.03	3.56	2.10+	1	1MGDBN
72 107H	85025	*	0.25	----	----	1	1MGBN
73 108H	77120	*	0.25	----	----	1	1MGBN
74 109H	86400	*	0.25	----	----	1	1LTJN
75 110HT	6440	*	0.25	----	----	1	1LGCN
76 105H	12560/1256	0.1	10	4.13	0.30	10000000	1ROY
89 111H	12550/1255	0.1	15	3.40	0.43	20500167	1MGDAY
91 113H	30000/3000	0.1	1	3.85	0.73	16100	1MGDBY
92 114H	21810/2181	0.1	10	3.48	0.60	69425	1MGDAY

95	115H	23590/2359	0.1	10	2.99	0.76	11417	1MGDAY
192	116H	-62482	*	0.25	----	----	1	1MGEN
193	117H	-61582	*	0.25	----	----	1	1MGEN
221	117H	-51082	*	1.2	----	----	1	1MGEHN
241	133H	20000/2000	0.1	15	----	----	1401491	1UTN
242	137H	20000/2000	0.1	15	----	----	5420000	1RON
243	136H	25000/2500	0.1	10	----	----	502598	1UTBN
244	131H	25000/2500	0.1	10	----	----	1104989	1MGBN
245	132H	30000/3000	0.1	10	3.60	0.66	96327	1UTN
246	135H	30000/3000	0.1	10	3.63	0.63	79610	1LGN
247	130H	35000/3500	0.1	10	3.73	0.95	15703	1UTN
248	139H	40000/4000	0.1	5	3.37	1.20	2921	1LTAN
249	143H	40000/4000	0.1	5	4.01	1.04	1668	1MGAN
250	140H	50000/5000	0.1	5	3.39	1.53	742	1MGAN
253	149H	20000/2000	0.1	20	3.45	0.57	8222998	1LTN
254	150H	20000/2000	0.1	15	----	----	11500000	1RON
258	118H	102555	*	0.25	3.51	----	1	1MGBN
259	150H	106338	*	0.25	4.01	----	1	1MGBN
260	151H	107947	*	0.25	4.17	----	1	1MGBN
269	125H	97000	*	0.25	3.51	----	1	1MGBFY
270	128H	95182	*	0.25	3.63	----	1	1MGBFY

SUMMARY OF FIBERGLASS FATIGUE RESULTS MATERIAL J

TEST & SAMPLE ID #	STRESS PSI	R	Q Hz	E MSI	e %	CYCLES TO FAIL	FAILURE MODE
62 101J	63590	*	1.0	3.56	3.23+	1	1MGDBY
63 102J	54235	*	1.0	3.44	1.6	1	1MGDBY
65 103J	----	*	1.0	----	----	1	1MGDB
68 104J	25050/2505	0.1	5	3.45	0.77	17882	1MGDBY
70 105J	12500/1250	0.1	10	3.80	0.31	11000000	1ROY
81 106J	10770/1077	0.1	15	3.28	0.26	18000000	1ROY
82 107J	10910/1091	0.1	15	3.96	0.28	30300000	1ROY
93 108J	18000/1800	0.1	10	3.35	0.54	153500	1ROY
94 109J	27230	*	--	3.27	0.82	1	1ROEY
127 110J	15000/1500	0.1	15	3.51	0.42	1460000	1MGDBY
194 111J	-58396	*	0.25	----	----	1	1MGEN
195 112J	-60448	*	0.25	----	----	1	1MGEN
220 113J	----	*	1.2	----	----	1	1MGBX
261 140J	104793	*	0.25	3.81	----	1	1MGBN
262 141J	103183	*	0.25	3.73	----	1	1MGBN
263 142J	99863	*	0.25	3.51	----	1	1MGBN
268 115J	97139	*	0.25	3.55	----	1	1MGBFY

SUMMARY OF FIBERGLASS FATIGUE RESULTS MATERIAL L

TEST & SAMPLE ID #	STRESS PSI	R	Q Hz	E MSI	e %	CYCLES TO FAIL	FAILURE MODE
77 101L	59480/5948	0.1	1	5.13	1.18	2580	1UGB
78 103L	58820/5882	0.1	1	4.48	1.32	593	1UGB
79 102L	40000/4000	0.1	5	4.57	0.87	59081	1MGB
80 104L	38550/3855	0.1	5	4.21	0.97	45848	1UGB

83	109L	47120/4712	0.1	10	5.00	0.91	153402	1UTJ
84	127L	4/3.5/3.75K	0.1	10	4.70	0.93	450000	1RO
101	117L	107260	*	0.25	4.47	2.40	1	1MGB
102	119L	108053	*	0.25	5.31	2.21	1	1MGB
196	122L	-47161	*	0.25	----	----	1	1MGE
197	123L	-48207	*	0.25	----	----	1	1MGE
198	125L	-47515	*	0.25	----	----	1	1MGE
199	126L	-50836	*	0.25	----	----	1	1MGE
231	126L	-52369	*	0.1	----	----	1	1MGEV
232	127L	-64333	*	0.25	----	----	1	1MGEV
233	128L	-60360	*	0.25	----	----	1	1MGEV

SUMMARY OF FIBERGLASS FATIGUE RESULTS MATERIAL M

TEST & SAMPLE ID #	STRESS PSI	R	Q Hz	E MSI	e %	CYCLES TO FAIL	FAILURE MODE	
129	101M	10000/1000	0.1	15	3.11	0.32	17764694	2MGDB
130	102M	11000/1100	0.1	15	3.05	0.36	6899599	2MGB
131	104M	76146	*	2.4	3.04	3.0	1	2MGB
132	113M	73523	*	2.4	2.93	2.9	1	2MGB
133	112M	20000/2000	0.1	10	3.13	0.66	18650	2MGBD
134	106M	20000/2000	0.1	10	3.07	0.66	22360	2MGB
135	109M	30000/3000	0.1	5	2.80	1.12	2319	2UGB
136	103M	30000/3000	0.1	5	2.77	1.12	2855	2MGB
137	114M	40000/4000	0.1	5	2.90	1.43	687	2LGB
138	105M	40000/4000	0.1	5	2.79	1.44	879	2LGB
139	115M	15000/1500	0.1	15	3.04	0.49	86249	2MGB
140	107M	15000/1500	0.1	15	3.03	0.49	174168	2MGA
141	118M	12500/1250	0.1	15	2.97	0.41	397000	2MGB
142	110M	12500/1250	0.1	15	3.25	0.39	266000	2MGA
143	108M	11000/1100	0.1	15	3.10	0.36	2498512	2LTJ
200	124M	-39824	*	0.25	----	----	1	2MGE
201	123M	-42816	*	0.25	----	----	1	2MGE
202	122M	-41964	*	0.25	----	----	1	2MGE
203	125M	-41185	*	0.25	----	----	1	2MGE
228	126M	-38765	*	0.1	----	----	1	2MGEV
229	127M	-42143	*	0.25	----	----	1	2MGEV
230	128M	-43636	*	0.25	----	----	1	2MGEV

SUMMARY OF FIBERGLASS FATIGUE RESULTS MATERIAL N

TEST & SAMPLE ID #	STRESS PSI	R	Q Hz	E MSI	e %	CYCLES TO FAIL	FAILURE MODE	
85	111NT	12410	*	0.25	----	3.3	1	1UGC
86	101NT	7785/779	0.1	1	1.25	1.34	6479	2UGC
87	102NT	9800/980	0.1	1	1.14	1.7	470	2MGC
88	104NT	5000/500	0.1	5	1.24	0.45	511047	2UGC
96	103NT	3000/300	0.1	15	3.35	0.28	34000000	2RO
103	011N	69850	*	0.25	3.03	2.97	1	1MGB
104	012N	67850	*	0.25	3.03	2.84	1	1MGB
105	113NT	12600	*	0.25	1.00	3.82	1	1UGB
106	114NT	13050	*	0.25	1.33	2.29	1	1MGB

109	111NT	7785/779	0.1	1	1.28	1.15	7950	2UGB
110	112NT	9800/980	0.1	1	0.97	1.42	711	2UGB
111	117N	56270/5627	0.1	1	2.47	2.74	27	1UGB
112	116N	40000/4000	0.1	1	2.64	1.60	626	1UGB
113	120N	40000/4000	0.1	5	2.51	1.70	811	1LGB
114	114NT	5000/500	0.1	15	1.19	0.42	1634579	2LGCB
115	118N	30000/3000	0.1	15	2.78	1.08	5684	1MGJDB
116	119N	30000/3000	0.1	5	2.85	1.05	4871	1UGDB
117	010N	20000/2000	0.1	10	2.92	0.69	25371	2LGA
118	009N	20000/2000	0.1	10	2.83	0.71	25781	2LGCB
119	129N	20000/2000	0.1	10	2.96	0.68	37597	2UGJDB
120	128N	20000/2000	0.1	10	2.78	0.72	29230	2LGDB
121	131N	15000/1500	0.1	15	2.67	0.56	231826	2MGA
122	130N	12500/1250	0.1	15	2.87	0.42	1336695	2UGA
123	006N	50000/5000	0.1	1	2.78	1.82	150	2MGB
124	126N	11000/1100	0.1	15	2.85	0.39	1648137	2MGDB
125	008N	10000/1000	0.1	15	2.89	0.34	7825000	2MGA
126	121N	15000/1500	0.1	15	2.75	0.54	165980	2MGDB
128	127N	10000/1000	0.1	15	2.80	0.35	4005593	2UGCB
145	116N	66933	*	2.4	2.93	2.81	1	2MGB
146	117N	66599	*	2.4	2.74	2.75	1	2MGB
208	151N	-46055	*	0.25	----	----	1	2MGE
209	152N	-48384	*	0.25	----	----	1	2MGE
210	153N	-43725	*	0.25	----	----	1	2MGE

FAILURE LOCATION AND MODE DESCRIPTION MNEMONICS

A - STOPPED A FEW CYCLES FROM FAILURE
 B - BROOMING OF THE FIBERS
 C - CLEAN TRANSVERSE FRACTURE
 D - DEBONDING OF PLY LAYERS
 E - BUCKLING OF THE SAMPLE
 F - NET CROSS SECTION AREA
 H - 1/2 INCH HOLE IN SPECIMEN
 J - JAGGED TRANSVERSE FRACTURE
 LG - LOWER GAGE LOCATION
 LT - LOWER TAB LOCATION
 MG - MID GAGE LOCATION
 N - MATERIAL DOES NOT HAVE A JOINT
 RO - RUN OUT, NOT FAILED
 S - TAB DEBONDING FROM SAMPLE
 T - Included on sample ID # indicates a transverse test.
 UG - UPPER GAGE LOCATION
 UT - UPPER TAB LOCATION
 V - DOUBLE THICKNESS SAMPLE
 X - NOT A VALID TEST
 Y - MATERIAL HAS A JOINT
 1 - 1 INCH NOMINAL MATERIAL WIDTH
 2 - 2 INCH NOMINAL MATERIAL WIDTH

* = STATIC TEST - The test frequency "Q" is replaced by the "ramp rate" in inches per second. The initial strain is replaced by the strain at failure.

DISTRIBUTION:

Dr. R. E. Akins
Washington & Lee University
P.O. Box 735
Lexington, VA 24450

Dr. Mike Anderson
Renewable Energy Systems, Ltd.
Eaton Court, Maylands Avenue
Hemel Hempstead
Herts HP2 7DR
UNITED KINGDOM

Dr. M. P. Ansell
School of Material Science
University of Bath
Claverton Down
Bath BA2 7AY
Avon
UNITED KINGDOM

W. R. Archibald
FloWind Corporation
990 A Street, Suite 300
San Rafael, CA 94901

Holt Ashley
Dept. of Aeronautics and
Astronautics Mechanical Engr.
Stanford University
Stanford, CA 94305

K. Bergey
University of Oklahoma
Aero Engineering Department
Norman, OK 73069

Ir. Jos Beurskens
Programme Manager for
Renewable Energies
Netherlands Energy Research
Foundation ECN
Westerduinweg 3
P.O. Box 1
1755 ZG Petten (NH)
THE NETHERLANDS

N. Butler
Bonneville Power Administration
P.O. Box 3621
Portland, OR 97208

Dr. R. N. Clark
USDA
Agricultural Research Service
Southwest Great Plains Research
Center
Bushland, TX 79012

C. Coleman
Northern Power Systems
Box 659
Moretown, VT 05660

Otto de Vries
National Aerospace Laboratory
Anthony Fokkerweg 2
Amsterdam 1017
THE NETHERLANDS

E. A. DeMeo
Electric Power Research Institute
3412 Hillview Avenue
Palo Alto, CA 94304

J. B. Dragt
Institute for Wind Energy
Faculty of Civil Engineering
Delft University of Technology
Stevinweg 1
2628 CN Delft
THE NETHERLANDS

A. J. Eggers, Jr.
RANN, Inc.
260 Sheridan Ave., Suite 414
Palo Alto, CA 94306

John Ereaux
RR No. 2
Woodbridge, Ontario L4L 1A6
CANADA

Jim Frerotte
Phoenix Industries
1200 Bruce Street
P.O. Box 455
Crookston, MN 56716

A. D. Garrad
Garrad Hasson
9-11 Saint Stephens Street
Bristol BS1 1EE
ENGLAND

P. R. Goldman
Wind/Hydro/Ocean Division
U.S. Department of Energy
1000 Independence Avenue
Washington, DC 20585

W. B. Goldsworthy
27520 Hawthorne Blvd., Suite 240
Rolling Hills Estates, CA 90274

Dr. I. J. Graham
Dept. of Mechanical Engineering
Southern University
P.O. Box 9445
Baton Rouge, LA 70813-9445

Professor N. D. Ham
Aero/Astro Dept.
Massachusetts Institute of
Technology
77 Massachusetts Avenue
Cambridge, MA 02139

Loretta Helling
Librarian
National Atomic Museum
Albuquerque, NM 87185

W. E. Holley
U.S. WindPower
6952 Preston Avenue
Livermore, CA 94550

M. A. Ilyan
Pacific Gas and Electric Co.
3400 Crow Canyon Road
San Ramon, CA 94583

K. Jackson
Dynamic Design
123 C Street
Davis, CA 95616

O. Krauss
Division of Engineering Research
Michigan State University
East Lansing, MI 48825

V. Lacey
Indal Technologies, Inc.
3570 Hawkestone Road
Mississauga, Ontario L5C 2V8
CANADA

G. G. Leigh
New Mexico Engineering
Research Institute
Campus P.O. Box 25
Albuquerque, NM 87131

L. K. Liljegren
120 East Penn Street
San Dimas, CA 91773

R. R. Loose, Director
Wind/Hydro/Ocean Division
U.S. Department of Energy
1000 Independence Ave., SW
Washington, DC 20585

Robert Lynette
R. Lynette & Assoc., Inc.
15042 NE 40th Street
Suite 206
Redmond, WA 98052

Peter Hauge Madsen
Riso National Laboratory
Postbox 49
DK-4000 Roskilde
DENMARK

David Malcolm
R. Lynette & Associates, Inc.
15042 N.E. 40th Street, Suite 206
Redmond, WA 98052

Prof. J. F. Mandell (25)
Montana State University
302 Cableigh Hall
Bozeman, MT 59717

Bernard Masse
Institut de Recherche d'Hydro-Quebec
1800, Montee Ste-Julie
Varennes, Quebec J3X 1S1
CANADA

Gerald McNERNEY
U.S. Windpower, Inc.
6952 Preston Avenue
Livermore, CA 94550

R. N. Meroney
Dept. of Civil Engineering
Colorado State University
Fort Collins, CO 80521

Alan H. Miller
NREL
1617 Cole Boulevard
Golden, CO 80401

R. H. Monroe
Gougeon Brothers
100 Patterson Avenue
Bay City, MI 48706

D. Morrison
New Mexico Engineering
Research Institute
Campus P.O. Box 25
Albuquerque, NM 87131

V. Nelson
Department of Physics
West Texas State University
P.O. Box 248
Canyon, TX 79016

Dr. D. I. Page
Energy Technology Support Unit
B 156.7 Harwell Laboratory
Oxfordshire, OX11 ORA
UNITED KINGDOM

Chuck Paquette
The American Wind Energy Association
777 N. Capitol Street, NE
Suite 805
Washington, DC 20002

Troels Friis Pedersen
Riso National Laboratory
Postbox 49
DK-4000 Roskilde
DENMARK

Helge Petersen
Riso National Laboratory
Postbox 49
DK-4000 Roskilde
DENMARK

Raj Rangi
Manager, Wind Technology
Dept. of Energy, Mines and Resources
580 Booth 7th Floor
Ottawa, Ontario K1A 0E4
CANADA

Markus G. Real, President
Alpha Real Ag
Feldeggstrasse 89
CH 8008 Zurich
Switzerland

L. Schienbein
7080 Donlon Way, Suite 210A
Dublin, CA 94568

Thomas Schweizer
Princeton Economic Research, Inc.
12300 Twinbrook Parkway
Rockville, MD 20852

David Sharpe
Dept. of Aeronautical Engineering
Queen Mary College
Mile End Road
London, E1 4NS
UNITED KINGDOM

L. H. Soderholm
Agricultural Engineering
Room 213
Iowa State University
Ames, IA 50010

W. J. Steeley
Pacific Gas and Electric Co.
3400 Crow Canyon Road
San Ramon, CA 94583

Forrest S. Stoddard
West Texas State University
Alternative Energy Institute
WT Box 248
Canyon, Texas 79016

Derek Taylor
Alternative Energy Group
Walton Hall
Open University
Milton Keynes MK7 6AA
UNITED KINGDOM

G. P. Tennyson
DOE/AL/ETWMD
Albuquerque, NM 87115

Walter V. Thompson
410 Ericwood Court
Manteca, CA 95336

R. W. Thresher
NREL
1617 Cole Boulevard
Golden, CO 80401

K. J. Touryan
3701 Hawkins Street, NE
Albuquerque, NM 87109-4512

W. A. Vachon
W. A. Vachon & Associates
P.O. Box 149
Manchester, MA 01944

P. Vittecoq
Faculty of Applied Science
University of Sherbrooke
Sherbrooke, Quebec J1K 2R1
CANADA

T. Watson
Canadian Standards Association
178 Rexdale Boulevard
Rexdale, Ontario M9W 1R3
CANADA

L. Wendell
Battelle-Pacific Northwest
Laboratory
P.O. Box 999
Richland, WA 99352

M. Zuteck
MDZ Consulting
931 Grove Street
Kemah, TX 77565

1434	D. W. Lobitz
1434	D. R. Martinez
1511	G. F. Homicz
1514	J. G. Arguello
1514	H. S. Morgan
1540	J. R. Asay
1552	J. H. Strickland
1562	K. E. Metzinger
1562	E. D. Reedy
2741	T. G. Carne
2741	G. H. James III
2741	J. P. Lauffer
2741	R. Rodeman
6000	D. L. Hartley
6214	H. M. Dodd (50)
6214	T. D. Ashwill
6214	D. E. Berg
6214	S. C. Newton
6214	M. A. Rumsey
6214	L. L. Schluter
6214	W. A. Stephenson
6214	H. J. Sutherland (5)
6214	P. S. Veers
7141	S. A. Landenberger (5)
7151	G. C. Claycomb (3)
7613-2	Document Processing (8) For DOE/OSTI
8523-2	Central Technical Files